

Received 19 May 2025, accepted 19 June 2025, date of publication 25 June 2025, date of current version 2 July 2025.

Digital Object Identifier 10.1109/ACCESS.2025.3583080

RESEARCH ARTICLE

LEO-PNT Feasibility Aspects: Satellite Navigation Payload Size, Weight, and Power Analysis

MAYANK¹, F. S. PROL^{2,3}, V. LUNDÉN¹, Z. SALEEM¹,
GUILLEM FOREMAN-CAMPINS (Graduate Student Member, IEEE),⁴
S. SHARMA¹, E. S. LOHAN⁴, (Senior Member, IEEE), M. Z. H. BHUIYAN²,
S. KAASALAINEN², H. KUUSNIEMI^{2,4}, (Member, IEEE), AND J. PRAKS¹, (Member, IEEE)

¹Department of Electronics and Nanoengineering, Aalto University, 02150 Espoo, Finland

²Department of Navigation and Positioning, Finnish Geospatial Research Institute (FGI), National Land Survey of Finland (NLS), 02150 Espoo, Finland

³School of Technology and Innovations, University of Vaasa, 65101 Vaasa, Finland

⁴Tampere Wireless Research Centre, Tampere University, 33720 Tampere, Finland

Corresponding author: Mayank (mayank@aalto.fi)

This work was supported in part by the INdoor Navigation from the CUBesAT Technology (INCUBATE) Project coordinated by the University of Vaasa, in part by the Building the Future-Taking Action Initiative funded by the Centennial Foundation of the Federation of Finnish Technology Industries and the Jane and Aatos Erkkö Foundation, in part by the LED Disinfection and Solar Energy Utilization Project (LEDSOL) Project funded under the Long-Term Joint EU-AU Research and Innovation Partnership on Renewable Energy (LEAP-RE) Program through European Union's Horizon 2020 Research and Innovation Program under Grant 963530, and in part by the Academy of Finland under Grant 352364.

ABSTRACT Low Earth Orbit (LEO) satellites are expected to improve the robustness and reliability of critical Positioning, Navigation, and Timing (PNT) services by increasing both the efficiency and diversity of Global Navigation Satellite Systems (GNSS). However, the feasibility of LEO-PNT services remains uncertain primarily due to the large number of required satellites. The deployment of a LEO-PNT system therefore depends on the feasibility of deploying many LEO satellites with characteristics strongly dependent on the performance requirements of both the payload and the platform. This work addresses the feasibility uncertainty by modeling two potential LEO-PNT payloads and satellite platform designs with different size, weight, and power (SWaP) requirements. Based on simulations and components currently available in the space market, a holistic modeling for the performance of low- and high-SWaP payload designs is evaluated with a focus on clock stability and signal quality. Additionally, the design process includes an assessment of a custom navigation antenna to ensure that the antenna can meet its stringent size and performance constraints. The feasibility of the proposed LEO-PNT constellations is evaluated based on satellite link, power, and mass budgets, as well as antenna performance. In addition, the cost of both the low- and high-SWaP satellites is estimated. This work shows that LEO-PNT payload and constellations are feasible with the technology commercially available today, and they could offer significantly stronger PNT signals compared to traditional GNSS services. The work also benchmarks the proposed payloads against commercial projects in terms of SWaP, timing and positioning accuracy. These results can assist future LEO-PNT simulations to utilize detailed information of payload components and take LEO-PNT services a step closer to realization.

INDEX TERMS Constellation, feasibility study, LEO-PNT, navigation.

I. INTRODUCTION

In recent years, envisioned low Earth orbit (LEO) satellites dedicated for positioning, navigation, and timing (PNT) have been showing increasing potential [1], [2], [3]. Although a military funded LEO-PNT constellation was first

demonstrated already in the 1960s in the US [4], today the miniaturization of satellites with modern technology has the potential to enable unprecedented LEO-PNT performance. However, one of the main challenges in the development of the emerging modern LEO-PNT technologies is finding a feasible and cost-effective concept design [5]. It is uncertain whether LEO-PNT systems would enhance Global Navigation Satellite Systems (GNSS) sufficiently to justify the

The associate editor coordinating the review of this manuscript and approving it for publication was Zhenbao Liu¹.

substantial transformation on how localization is performed today.

Traditionally, it is assumed that a functional LEO-PNT constellation offering global service requires hundreds of satellites [6], [7], [8], each equipped with heavy, power-intensive atomic clocks that enable transmitting navigation signals. However, more optimized solutions exist [9]. For instance, GNSS receivers onboard LEO satellites [10] can eliminate the need for heavy atomic clocks while maintaining sufficient medium-term stability. Additionally, by optimizing the LEO-PNT payload design, it is possible to refine navigation messages [11] and reduce the need for the extensive ground segment infrastructure typically required for classic GNSS. Furthermore, the reduced impact of free path loss [12] can allow less stringent platform requirements while still achieving satisfactory navigation signal power on ground.

The signal strength provided by LEO-PNT systems is expected to exceed that of traditional GNSS signals, offering enhanced reliability and resilience against both natural (e.g., ionospheric scintillation and multipath propagation) and intentional interference (e.g., jamming and spoofing). Typically, LEO-PNT design approaches utilize customized payload systems developed under proprietary regulations. For instance, [13] assumes that LEO-PNT payloads can operate with characteristics similar to those generating GNSS signals. Furthermore, [14] and [15] simulate data of Starlink and OneWeb satellites to understand the positioning improvements under multipath and urban canyons environments. Although such geometry simulations can be performed reasonably well, characteristics of the signal design are oversimplified unless demonstrated by payload developers, such as in [16], [17], and [18]. As a result, researchers often rely on simplified payload options to conduct LEO-PNT simulations.

The objective of this work is to propose a feasible LEO-PNT payload design. Given that the design of PNT payloads and satellites is heavily constrained by the SWaP budget of the system, this work presents two payloads with different PNT performance: a low- and high-SWaP option. To promote transparency, the LEO-PNT payloads designed in this work are based solely on components for which detailed open access information is readily available through the space market and scientific literature. In addition, a preliminary custom isoflux navigation antenna design is considered to estimate its effects on signal performance and constellation design. The final payload designs are the result of a comprehensive analysis of a wide range of key components. In addition to the detailed designs, this work analyzes signal performance of the proposed payloads without needing to resort to simplifications commonly required when payload details are unavailable.

In addition to the two payloads, this work presents two satellite system designs to support them. The low-SWaP PNT payload accompanied by a smaller spacecraft utilizes only a single navigation signal frequency, whereas the high-SWaP payload with the larger spacecraft can generate

navigation signals at two frequencies to enhance PNT signal performance. Both LEO-PNT satellite options are compared in terms of their link, mass, and power budgets, in addition to cost estimates. To complete the proposed LEO-PNT systems, a comprehensively analyses is presented regarding the constellation design.

This work significantly extends on previous work in the literature that overview the status of LEO-PNT systems [19], [20]. The previous work provides only a high-level overview of the LEO-PNT payload concept and preliminary component considerations, whereas this work presents a literature review and a novel in-depth analysis of the PNT payload and system based on an extensive component review and detailed performance analyses. The main contributions of this work are listed below:

- This work introduces a novel architecture for LEO-based PNT payloads specifically tailored for small satellite platforms.
- It includes a comprehensive survey of commercial off-the-shelf (COTS) components suitable for implementing the key functional modules of the proposed payloads.
- Two distinct payload configurations have been modeled for low and high SWaP requirements. Signal modeling to evaluate their C/N_0 of two L-band frequencies, timing accuracy, and link margins have been presented.
- Another key system, small satellite isoflux antenna and its radiation pattern has been modeled across different orbital altitudes and elevation angles. Signal modeling highlighting its impact on C/N_0 , constellation design and global coverage.
- Corresponding satellite bus designs are modelled for each payload configuration, demonstrating the impact of SWaP considerations and cost on overall satellite architecture.
- Benchmarking to validate the feasibility and competitiveness of the proposed LEO-PNT satellite in SWaP and navigation performance against several existing commercial LEO-PNT solutions has been presented.

To the best of the Authors' knowledge, none of the above-mentioned points have been addressed so far in the existing literature on LEO-PNT.

The rest of the work is structured as follows: Section II presents the driving requirements of the LEO-PNT payload design architecture. Section III presents the novel LEO-PNT payload architecture common for both the low- and high-SWaP payloads. Section IV provides the literature study of the potential instruments and components that can be used for the payload design. Section V presents the instruments and components selected for the payloads, as well as the two satellite designs for both payload options. In addition, it compares the estimated performance of the low- and high-SWaP systems and presents the proposed constellation design. Section VII discusses the payload performance analysis and compares the proposed systems with existing commercial LEO-PNT constellation concepts. Finally, Section VIII presents concluding remarks.

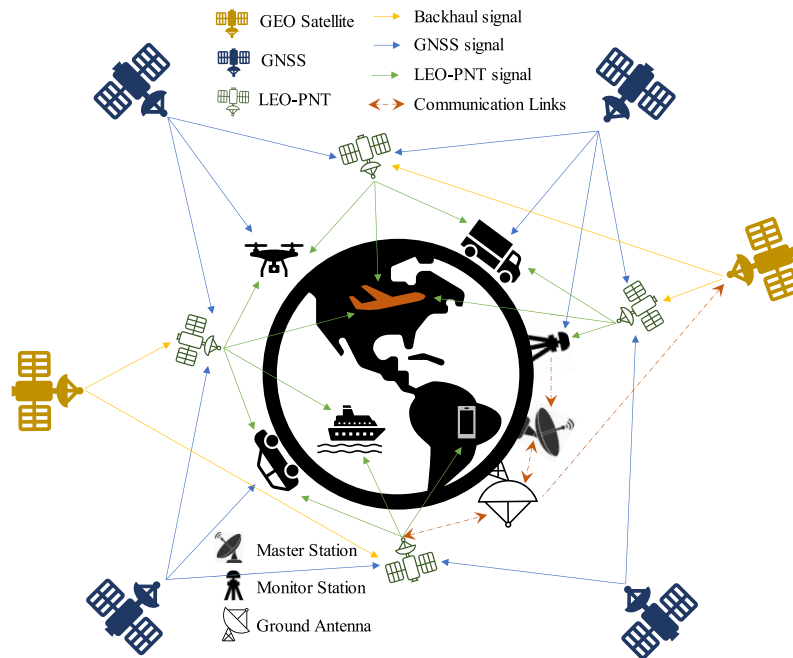


FIGURE 1. Overview of the proposed LEO-PNT mission concept. The LEO-PNT satellites (green) use signals and data from both GNSS satellites (blue) and geostationary satellites (yellow) to produce high-quality navigation messages that are subsequently transmitted to ground users.

II. PNT SYSTEM REQUIREMENTS

The high level requirements of the LEO-PNT system concept developed in this work are based on targeted service coverage, PNT service quality, and cost efficiency. These requirements and their justifications are the following:

- A minimum of four LEO-PNT satellites should be visible from any point within the coverage area at least 99% of the time. With fewer visible satellites, the positioning performance is significantly degraded.
- The coverage area shall range from 75°S to 75°N in terms of latitude. This range is sufficient to cover the main industrial geographical areas of the world [5]. In the rest of this work, this is referred to as “global coverage”.
- The clock accuracy of the LEO-PNT system shall in no case be worse than 1 ns. This limit is defined to ensure sufficient timing accuracy for PNT applications [21].
- The carrier-to-noise ratio of the LEO-PNT signals shall be higher than typical GNSS signals at all elevation angles. Through improved carrier-to-noise ratio, the LEO-PNT system can provide benefits such as better resilience against interference [22].
- The system shall demonstrate SWaP characteristics that can enable a mega-constellation. A LEO-PNT constellation offering global coverage requires a large number of satellites, and their miniaturization is critical in maintaining reasonable constellation cost.
- The integration between LEO-PNT and GNSS must be possible both in space and on ground. This ensures that

no costly infrastructure modifications are required for the LEO-PNT system to seamlessly supplement existing GNSS services.

These high-level requirements must be obeyed by both the low- and high-SWaP payloads and related satellite designs. The constellation design must also adhere to the relevant requirements to ensure sufficient global coverage.

III. CONCEPT DESIGN

A. LEO-PNT MISSION DESIGN

The mission concept proposed and analyzed in this work is illustrated in Fig. 1. It shows a dedicated LEO-PNT system where LEO satellites (shown in green) use signals from GNSS satellites (shown in blue) to estimate LEO satellite orbits and clock states with high precision. This information is combined with an initial navigation message received from backhaul satellites (shown in yellow) in geostationary orbit (GEO). An enhanced navigation message is then computed onboard each LEO satellite and transmitted to ground terminals along with a PNT code. The transmitted PNT signal is designed to enable the retrieval of range measurements (e.g., pseudorange, carrier phase, and Doppler shift) along the ground-to-LEO line of sight. User terminals can then calculate positioning, velocity, and timing based on the received signal. Also, backhaul ground stations receive the LEO-PNT signals and estimates the state variables of the navigation messages. These state variables are subsequently transmitted back to the GEO backhaul satellites, closing the error detection and correction system loop.

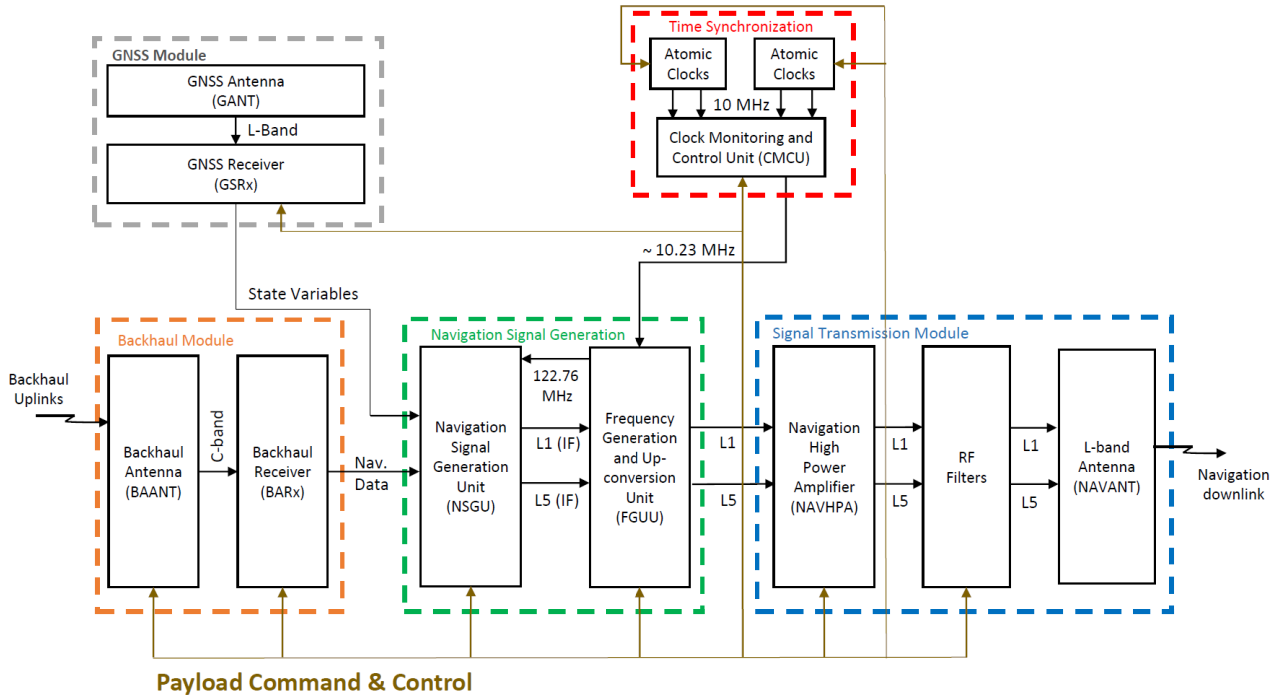


FIGURE 2. Block-level diagram of the proposed LEO-PNT payload architecture. The system can be divided into five high-level modules: a time synchronization module, a GNSS module, a backhaul module, a navigation signal generation module, and a signal transmission module.

B. LEO-PNT PAYLOAD ARCHITECTURE

Fig. 2 illustrates a block-level diagram of the payload envisioned for the LEO-PNT system. The LEO-PNT payload is designed with a minimalist approach. The payload is composed by five modules: 1) a time synchronization module (TSM), that provides the clock time standard with a fundamental frequency of 10.23 MHz; 2) a GNSS module, containing a GNSS antenna and receiver for processing GNSS signals; 3) a backhaul module, containing a communication antenna and receiver; 4) a navigation signal generation module consisting of a signal generation unit (SGU) and a frequency generation and up-conversion unit (FGUU); and 5) the signal transmission module, including two power amplifiers, radio frequency (RF) filters, and a passive antenna in the L-band. A high level description of the modules is given below:

- **Time synchronization module:** Contains the atomic clocks for time synchronization across several modules.
- **GNSS module:** Responsible for the LEO satellite orbit determination and time synchronization in real-time. Outputs state variables, such as satellite position, velocity, acceleration, clock states, and associated co-variances.
- **Backhaul module:** Responsible for receiving an initial navigation message sent by the GEO satellites. The initial navigation message contains clock correction models, orbit models, ionospheric models, instrumental biases, quality indicators, and any additional corrections necessary for the user segment. They are estimated

by the ground segment and spread through the GEO backhaul satellites.

- **Navigation signal generation module:** Generates the refined LEO-PNT navigation signal modulated with the navigation messages in a specific carrier frequency.
- **Signal transmission module:** Contains the RF front-end and an antenna array for signal transmission.

The proposed LEO-PNT system presents several key differences compared to traditional GNSS payloads. The most prominent difference is found in the security unit. GNSS satellites often include a security unit to provide encrypted PNT signals for military usage. This unit is neglected in our development.

The time synchronization module design also presents relevant changes. In typical GNSS payloads, four heavy atomic clocks work in redundancy, and a dedicated clock monitoring and control unit (CMCU) is used to interface the atomic clocks and to guarantee an accurate fundamental frequency 10.23 MHz. The LEO-PNT payload designed in this study, in contrast, can rely in more simplified CMCU instruments, such as external computers, or even relies on using oscillators directly as the input time source, with no redundancy. This is justified under the assumption that the GNSS receiver will continuously provide clock corrections to synchronize the atomic clock with the correct atomic time. In other words, although the atomic clock can drift over time, clock corrections provided by GNSS are utilized for time synchronization. The feasibility, therefore, mainly depends on the capability of the atomic clock to keep the

short-term stability and the ability of the system to transmit clock corrections to the users.

Whereas MEO GNSS satellites utilize large antennas, the limited LEO satellite size leads to challenges in antenna design. For instance, Galileo uses around 45 stacked patch antennas (with a total diameter of 1.4 m and mass less than 15 kg) to provide a beam angle of around 8 degrees, enabling sufficient service coverage from MEO [23]. The navigation antennas required by the designed LEO-PNT mission must offer an isoflux radiation pattern with a 100° field-of-view to provide evenly distributed power and global coverage while allowing to maintain a reasonably low number of satellites in the constellation.

Based on the proposed payload architecture, the primary differences between the low- and high-SWaP payload designs are found in the time-synchronization module and the signal generation and signal-transmission modules. The low-SWaP and high-SWaP time-synchronization modules present short-term and medium-term dependency on MEO GNSS signals, respectively. That is, in the low-SWaP payload, the time synchronization module depends more frequently on the MEO GNSS signals for clock synchronization than the corresponding high-SWaP module. In terms of the signal generation and transmission modules, the low-SWaP modules produce only a single frequency navigation signal, whereas the high-SWaP modules offer dual-frequency navigation signals to improve PNT service. Single-frequency signal generation on the low-SWaP payload reduces the power amplifier requirements of the satellite, which in turn reduces the SWaP significantly. We have chosen the L1 and L5 bands to meet specifications similar to those currently used in GNSS satellites and upcoming LEO-PNT systems.

IV. POTENTIAL INSTRUMENTS AND COMPONENTS FOR THE PAYLOAD

In this section, various types of instruments and components that can be used to implement the payloads are evaluated and compared. The main objective is to examine the available options in terms of accuracy, size, mass, and power requirements, providing an overview of their main characteristics based on real and commercially available instruments. The presented values are average values obtained from the analysis of multiple instruments or components, and represent the typical characteristics of the the class of items in question.

A. TIME SYNCHRONIZATION MODULE

The overall performance of the LEO-PNT system payload depends heavily on the performance of the onboard atomic clock. There are several options for atomic clocks. More than 10 different atomic clocks were reviewed and compared. Table 1 presents their main characteristics in terms of type, size, power consumption, mass, and expected accuracy (Allan deviation). The chip scale atomic clocks (CSACs) presents the lowest SWaP with a power consumption of only 120 mW, and a mass of just 35 g. However, it provides also the poorest frequency standard stability. In contrast, rubidium atomic

frequency standard (RAFS) clocks are heavier and larger, with a power consumption of 60 W. Miniaturized ultra-stable oscillators (USOs) based on quartz crystals have a SWaP between CSAC and RAFS clocks with a power demand of 8 W. Passive hydrogen masers (PHMs) are the most bulky, heavy, and power-intensive systems, requiring up to 60 W of power. The most stable clocks in the short term 1 s to 10 s are USOs, while PHMs offer greater medium-term 1000 s to 10 000 s stability.

In addition to the atomic clocks, the time synchronization module requires a clock monitoring and control unit. Considering that the task of the CMCU is to act as a signal processor, verifying the stability of the clocks, and deciding on the most stable frequency, the CMCU can be based on graphical processing units (GPUs), central processing units (CPUs), or field-programmable gate arrays (FPGAs). Another, more traditional option in GNSS satellites is the use of master clock units. These units help maintain a more stable interface between the clocks and can even improve their stability. Comparing these options, FPGAs are most energy-efficient, as they are implemented on hardware-level to solve specific tasks. GPUs, on the other hand, offer superior processing speed, while CPUs allow for the execution of various tasks in parallel. For master clock units, the available market options present orders of magnitude larger size and higher weight compared to the other options, making them poorly suitable for small LEO-PNT satellites. Table 2 compiles the four different CMCU technology options for SWaP comparison.

B. GNSS MODULE

The GNSS module consists of at least one antenna and a GNSS receiver. In this work, more than 50 GNSS receivers have been reviewed. Table 3 describes the main characteristics of different types of GNSS receivers that could potentially be used on LEO platforms. In addition to SWaP, the table presents the number of channels and the accuracy of the receivers. The receivers included in the comparison are commercially available or have recently been analyzed by academic researchers.

Although selected receiver studies utilize similar evaluation criteria to define accuracy, i.e., real-time positioning solutions with three-dimensional (3D) 1σ accuracy, it should be noted that the accuracy in each study depends not only on the receiver but also on the algorithm implemented for precise orbit determination (POD). Therefore, the values presented do not fully describe the expected accuracy of the receivers but can provide a general guideline on the available solutions. In the future, system performance improvements could be achieved by incorporating POD augmentation systems, such as the use of corrections from Galileo high accuracy services (HAS) [33]. Furthermore, the receivers studied in this work are not all customized for LEO-PNT. More customized systems, such as the custom ATOMIC device [34], could potentially improve LEO-PNT payload performance even further.

Furthermore, this work considers the potential use of receivers dedicated for integration with software-defined

TABLE 1. Potential atomic clocks with their SWaP and stability performance on-board LEO-PNT satellites.

Type	Allan deviation				Size (mm)	Weight (g)	Power (W)	Ref.
	1 s	10 s	1000 s	10 000 s				
CSAC* (cesium)	3.0e−10	1.0e−10	3.0e−11	1.0e−11	40 × 35 × 11	35	0.12	[24]
Mini USO [§] (quartz)	2.0e−13	3.5e−13	5.0e−13	7.0e−13	60 × 60 × 32	250	8	[25]
USO [§] (quartz)	5.0e−13	5.0e−13	6.0e−13	-	132 × 120 × 105	2000	6.5	[26]
Mini RAFS [¶] (rubidium)	1.0e−11	3.0e−12	3.0e−13	1.0e−13	53 × 67.5 × 107	450	10	[27]
RAFS [¶] (rubidium)	3.0e−12	1.0e−12	3.0e−13	6.0e−14	217 × 124 × 117	3400	60	[27]
Mini PHM [‡] (hydrogen)	6.5e−13	1.4e−13	2.2e−14	7.0e−15	210 × 485 × 218	12 000	47–54	[28]
PHM [‡] (hydrogen)	1.8e−12	3.2e−13	2.2e−14	7.0e−15	210 × 500 × 250	18200	60–70	[29]

* chip-scale atomic clock, [§] ultra-stable oscillator, [¶] rubidium atomic frequency standard, [‡] passive hydrogen maser

TABLE 2. Potential CMCUs on-board LEO-PNT satellites.

Type	Size (mm)	Weight (g)	Power (W)	Ref.
GPU*	16 × 16	2	5–20	[30]
CPU [†]	29 × 29	2	33	[31]
FPGA [§]	45 × 45	2	15	[32]
Master clock unit	270 × 216 × 137	5200	21	[33]

* graphical processing unit

[†] central processing unit

[§] field-programmable gate array

radios (SDRs). This type of integration represents one of the most prominent solutions for developing customized payloads for LEO-PNT, as the SDR could function both as an SGU and a backhaul receiver. However, currently available GNSS/SDR options on the market exhibit relatively low accuracy, a problem that can be addressed by increasing the SWaP of the system.

Multiple GNSS antennas were studied. The typical characteristics of some GNSS antennas applicable for LEO-PNT systems are listed in Table 4. The GNSS antenna selection depends on several factors, including the orbit of the satellite (which affects the desired antenna radiation pattern and gain), the area or volume available for the antenna, and the targeted GNSS frequencies. Patch antennas are usually preferred for GNSS applications due to their low directivity, simple design, and compact size even at L-band frequencies, but other options exist as well. Cup-type antennas, excited by a patch element, present better gain performance and wider beamwidth than a patch alone, but require more space on the platform. The extended patch excited cup allows further reducing interference arising e.g. from multipath, but at the cost of even larger size and more weight. The conical log spiral antenna type requires the largest volume of the considered options.

C. NAVIGATION SIGNAL GENERATION MODULE

The navigation signal generation module, consists of a signal generator unit and a frequency generation and up-conversion

unit. The navigation messages are generated by the SGU that can be based on GPUs, CPUs, or FPGAs. These processors are similar to those presented for the CMCU in Section IV-A and can be implemented as integrated units. Table 5 presents a SWaP comparison of the processor options for the SGU.

The FGUU implementation has several different options. A total of 20 different commercial off-the-shelf (COTS) options were considered for FGUU. Different options based on underlying technologies are compiled in Table 6. The FGUU can utilize COTS components based on oscillators, application specific integrated circuits (ASICs), signal generators, upconverters, or frequency synthesizers. These technologies can easily work with external clock signals of 10 MHz. In general, all candidate technologies can output signals in a wide L-band frequency range and present low power consumption. However, ASICs and frequency synthesizers are lightweight and smaller in size compared to other FGUU instrument options.

D. BACKHAUL MODULE

The backhaul module, responsible for receiving the backhaul messages from GEO satellites, can be based on a wide range of different options. Many possible options were considered and studied for backhaul module. These options, including transponders, transceivers, receivers, SDRs, and GNSS-integrated receivers, are compiled in Table 7. Among these, SDRs stand out because of the wide variance in the weight, power consumption, and frequency ranges of SDR options. C-band instruments are less common for satellite operations, and therefore, the available options may not be fully certified for this use. On the other hand, S-band receivers are widely utilized in LEO satellite communications, offering a combination of lower weight, low power consumption, and detailed information on transmission rates. K/Ka-band instruments, in contrast, tend to be heavier and consume more power. The spread spectrum transponder selected for comparison presents high weight and power consumption compared to the other technologies. This is because the spread-spectrum transponder is designed for GEO satellites and it provides high interference resilience.

TABLE 3. Potential GNSS receivers on-board LEO-PNT satellites.

Type	Size (mm)	Weight (g)	Power (W)	No. channels	3D error (m)	Ref.
Chip-scale	40 × 40 × 10	1–60	0.1–1	60–500	5–10	[35], [36]
Commercial	100 × 100 × 50	60–1200	1–8	20–100	2–4	[37]
Dual receiver (GNSS/SDR)	96 × 96 × 15	450	6.5	60	4	[38]
High-grade	200 × 200 × 100	1200–7000	10–60	12–50	0.2–1	[39], [34]
Customized	47.5 × 70 × 10	27	1	554	0.2–1	[40]

TABLE 4. Potential GNSS antennas on-board LEO-PNT satellites.

Type	Size (mm)	Weight (g)	Gain (dBi)	Key properties	Ref.
Patch	100 × 100 × 15	130	0	Dual frequency, RHCP, wideband	[41]
Stacked patch	80 × 80 × 19	73	−1.3–4.4	Dual frequency, RHCP, narrow beam angle	[42]
Conical log spiral	220 × 220 × 220	454	0	Dual frequency, RHCP, TBC	[43]
Patch excited cup	160 × 160 × 55	325	7–9	Dual frequency, RHCP, TBC	[44]
Extended patch excited cup	200 × 200 × 85	735	8–9	Dual frequency, RHCP, low multipath interference	[44]

TABLE 5. Potential SGU processors for signal generatoin module on-board LEO-PNT satellites.

Type	Size (mm)	Weight (g)	Power (W)	Ref.
GPU*	16 × 16	2	5–20	[30]
CPU†	29 × 29	2	33	[31]
FPGA‡	45 × 45	2	15	[32]

*graphical processing unit

†central processing unit

‡field-programmable gate array

Different backhaul antennas options based on operational frequencies were compiled during this study. Antenna options for the backhaul module are presented in Table 8. All of them exhibit similar characteristics in terms of size and weight, with a trend towards smaller and lower profile antennas for higher frequencies. Since, backhaul receiver in some payload design options could also receive signals from ground command centers. The selection of the backhaul receiver and antenna is in the end heavily dependent on the chosen frequency band. The key characteristics of the different frequency bands are described in the following:

- **S-Band:** High resistance to atmospheric absorption and rain. Great coverage. Lower data transmission capacity that at higher frequency bands.
- **C-Band:** Moderate resistance to atmospheric absorption and rain. Moderate coverage. Moderate data transmission capacity. Subject to greater regulation for allocation.

- **K/Ku Bands:** Low resistance to atmospheric absorption and rain. Less coverage. High data transmission capacity.

E. TRANSMISSION MODULE

The backbone of the navigation signal transmission module is comprised of power amplifiers. More than 30 different power amplifiers for L-band frequency were studied and compared. Table 9 presents potential power amplifier options for the module based on leading underlying technologies. Gallium arsenide (GaAs) technology has been used for power amplifiers for many years at microwave frequencies and operates at 10 V or 15 V. Laterally-diffused metal-oxide semiconductor (LDMOS) technology based on silicon operates at 50 V and has been widely used in telecommunications [63]. Silicon LDMOS technology is primarily useful at frequencies below 4 GHz, making it suitable for L-band LEO-PNT applications. However, the emergence of gallium nitride (GaN) technology, operating from 28 V to 50 V on a low-loss and high thermal conductivity substrate like silicon carbide (SiC), can offer a more robust solution for space applications. GaN technology is suitable for operations below 6 GHz and, therefore, is also appropriate for LEO-PNT applications.

To provide constant signal power throughout the wide ground area covered by each satellite, isoflux antennas are needed. Isoflux antennas compensate for the more significant signal attenuation at lower elevation angles (caused by the increased signal path length and atmospheric attenuation) by providing higher gain off-nadir. Fig. 3 illustrates the shape and main characteristics of nadir-centered isoflux patterns. From Fig. 4, it can be seen that at an 800 km orbit altitude, the

TABLE 6. Potential FGUs on-board LEO-PNT satellites.

Type	Input frequency (MHz)	Output frequency (MHz)	Size (mm)	Weight (g)	Power (W)	Ref.
Oscillator	100	1600–2000	100 × 180 × 30	850	5	[45]
ASIC	10	> 100	53 × 53 × 2.5	4	6	[46]
Signal generator	10	10–20 000	52 × 81 × 52	TBC	1	[47]
Upconverter	2–70	2–3000	89 × 63 × 25.4	209	3.6	[48]
Frequency synthesizer	10	600–1390	15 × 15 × 3.5	TBC	4	[49]

TABLE 7. Potential backhaul receivers on-board LEO-PNT satellites.

Type	Frequency (MHz)	Size (mm)	Weight (g)	Power (W)	Details	Ref.
S-band transponder	2000–2400	120 × 80 × 50	740	1–5	SC*, 4–64 kbps	[50]
S-band receiver	2000–2400	100 × 90 × 25	200–220	1.5–2	SC*, 4–64 kbps	[51], [52]
C-band transponder	4500–4800	90 × 96 × 40	400	3.5	non-SC*, 4–64 kbps	[53]
C-band receiver	5000–6000	150 × 80 × 30	425	4	non-SC*, 4–64 kbps	[54]
K/K _a -band transceiver	17 000–31 000	180 × 130 × 87	2200	10	SC*, 4–64 kbps	[55]
Software defined radio (SDR)	70–6000	100 × 100 × 30	240–750	3–10	SC*, 4–64 kbps	[56], [57]
Dual receiver (GNSS/SDR)	1175–1576	96 × 96 × 15	450	6.5	SC*, 4–64 kbps	[38]
Spread-spectrum transponder	S, C, X, K _u , and K _a bands	-	3600	25	SC* (GEO [†]) 4–64 kbps	[58]

*space certified, † geostationary orbit

TABLE 8. Potential antennas for the backhaul module on-board LEO-PNT satellites.

Type	Frequency (MHz)	Size (mm)	Weight (g)	Ref.
S-band antenna	2025–2290	85 × 85 × 12	140	[59], [60]
C-band microstrip patch array	5800–8200	100 × 100 × 3	45	[61]
K-band flat antenna	17 000–21 000	84 × 98 × 1	50	[62]
K _a -band flat antenna	27 000–31 000	51 × 51 × 1	50	[62]

TABLE 9. Potential power amplifiers for transmission module on-board LEO-PNT satellites.

Type	Frequency (MHz)	Gain (dBi)	Output power (dBm)	Size (mm)	Weight (g)	Power (W)	Ref.
GaAs*	1–2500	40	40	172 × 68 × 25	907	65	[64]
Silicon LDMOS [†]	1400–1500	14	52	130 × 60 × 20	260	42	[65]
GaN [§]	100–22 000	35	35	15 × 79 × 40	280	34	[66]

*gallium arsenide, †laterally-diffused metal-oxide semiconductor, §gallium nitride

isoflux field-of-view required for maximum ground coverage is 100° , assuming a minimum signal elevation angle of 30° at the ground station.

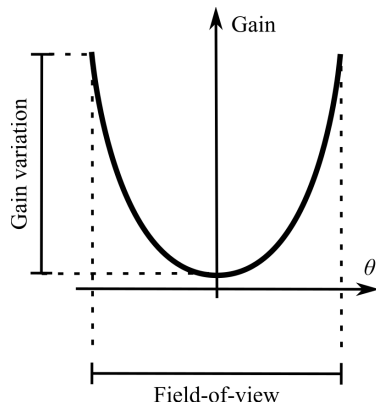


FIGURE 3. Illustrated 2D cut of an ideal nadir centered isoflux gain pattern. The gain is presented as a function of the beam angle θ . In 3D, the pattern would be rotationally symmetric around the gain axis in the figure.

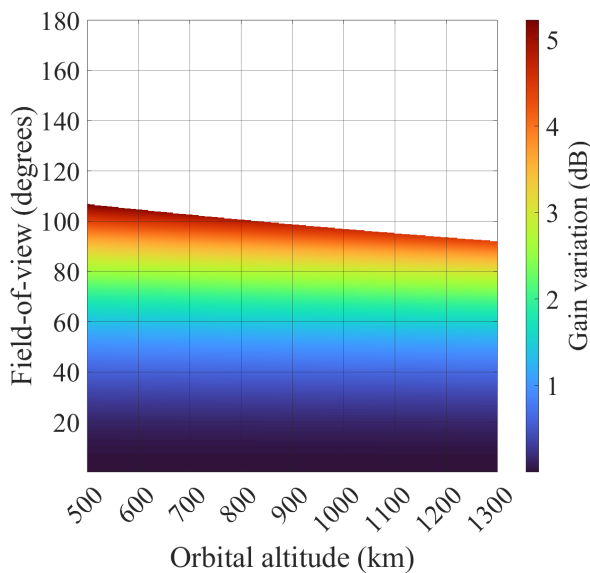


FIGURE 4. Gain variation within the field-of-view of an ideal isoflux pattern at L-band. The gain variation is presented as a function of the satellite orbital altitude and the antenna isoflux field-of-view. The upper bound for the field-of-view is set by the assumed ground terminal requirement of at least 30° signal elevation. For wider isoflux beams, the signal would reach ground from too low elevation angles near the edges of the pattern.

Because no viable commercial isoflux antennas were found on the market, custom isoflux antennas must be developed for the small satellites. In this work, a concentric ring array (CRA) is chosen as the custom isoflux antenna, because the utilization of CRAs for various isoflux radiation patterns has been extensively studied [67], [68], and they can produce isoflux radiation while maintaining compact size, low mass, and low complexity. The preliminary concept

antenna designed and modeled for this work based on [67] shows that CRA isoflux antennas can offer a nadir gain of at least 1 dB and provide better than 2 dB accuracy compared to the ideal isoflux pattern, while they maintain a compact form factor that fits a small satellite without requiring complex deployment systems. The key characteristics of the custom antenna are compiled in Table 10.

L-band has been chosen as the navigation frequency band for this feasibility study for two primary reasons. Firstly, many prominent LEO-PNT constellations already utilize the L-band for their navigation signals, ensuring compatibility and easing the integration of these new constellation services with existing ground receivers/infrastructure [5]. Secondly, the lower frequency of the L-band allows for a more conservative and practical antenna design, given the constraints on available dimensions. While we successfully demonstrate the feasibility of an L-band isoflux antenna, the findings also suggest that higher-frequency isoflux antennas could be implemented within the same form factor. However, the reverse—scaling a high-frequency design down to L-band—might not be as straightforward due to higher wavelength of L band as compared to other higher frequencies.

V. LEO-PNT SYSTEM CONCEPT AND FEASIBILITY

This section evaluates the feasibility of building a small satellite with the defined concept and potential instruments. The aim is to analyze the link margin, mass budget, and power budget of two proposed designs, a low-SWaP and a high-SWaP payloads. The two payload options are compared in terms of signal to noise ratio, long-term and short-term clock stability, SWaP requirements and the trade-offs of implementing a satellite platform capable of hosting the designed payloads. Furthermore, the estimated satellite SWaPs are compared with prominent LEO-PNT project satellites. In addition, this section analyzes constellation size and its global coverage considering antenna radiation pattern.

A. SELECTED INSTRUMENTS

The selection of the components and instruments for the low- and high-SWaP payloads is based on the options presented in Section IV. All instruments are real components and available on the market. The only exception is the custom L-band isoflux navigation antenna for which suitable commercial options were not found. The selected instruments for the low- and high-SWaP payloads are compiled in Table 11 and Table 12, respectively.

The proposed low- and high-SWaP payloads utilize 36 W and 77 W of power, respectively. The higher number of power amplifiers on the high-SWaP payloads is one of the primary reasons behind the higher power consumption of the whole payload. The high power consumption of the amplifiers enables the more than 30 dBm maximum transmission power needed for high-quality link to ground (the link budget is analyzed in more detail in Section V-B). For the atomic clock signal, the high-SWaP payload utilizes both a USO and an RAFS working in redundancy, providing better mid-term and short-term stability. The two clocks are synchronized

TABLE 10. Custom isoflux transmission compact antenna characteristics on-board LEO-PNT satellites.

Type	Nadir gain (dBi)	Frequency	Size (mm)	Weight (g)	Beamwidth (°)
Concentric ring array	1	L-band	300 × 300 × 5	350	100

TABLE 11. Instruments selected for the low-SWaP LEO-PNT payload. When multiple identical instruments are used, the size is given for a single unit, whereas the weight and power consumption are given as a total for all the units combined.

Module	Instrument	Size (mm)	Weight (g)	Power (W)
Time synchronization	Chip-scale atomic clock	41 × 35 × 11.4	0.35	0.12
GNSS module	COTS antenna	80 × 80 × 19	73	-
	Customized receiver	48 × 70 × 10	27	1
Signal generation	GPU	45 × 45 × 1	10	10
	frequency synthesizer	15 × 15 × 3.5	209	4
Backhaul	SDR receiver	100 × 100 × 30	240	3
Signal transmission	GaN power amplifiers (2) (1 active)	81 × 84 × 12	204	18
	RF filters (2)	9 × 35 × 8	10	-
	Custom isoflux antenna (1)	300 × 300 × 5	350	-
Total	10 units	-	1123	36

TABLE 12. Instruments selected for the high-SWaP LEO-PNT payload. When multiple identical instruments are used, the size is given for a single unit, whereas the weight and power consumption are given as a total for all the units combined.

Module	Instrument	Size (mm)	Weight (g)	Power (W)
Time synchronization	USO	60 × 60 × 32	250	8
	RAFS	53 × 68 × 107	450	10
GNSS module	COTS antenna	80 × 80 × 19	73	-
	Custom receiver	48 × 70 × 10	27	1
Signal generation	FPGA	45 × 45	10	15
	Frequency upconverters (2)	89 × 63.5 × 25	209	4
Backhaul	SDR receiver	100 × 100 × 30	240	3
Signal transmission	GaN power amplifiers (3) (2 active)	81 × 84 × 12	612	36
	RF filters (4)	9 × 35 × 8	40	-
	Custom isoflux antenna (2)	300 × 300 × 5	700	-
Total	16 units	-	2611	77

using onboard FPGA offering dual functionality of clock monitoring unit as well as navigation signal generator. The low-SWaP system, in contrast, is designed with a CSAC, focusing only on short-term stability, and relying heavily on GNSS signals for time corrections. The low- and high-SWaP payloads are 1.1 kg and 2.6 kg respectively. The mass difference is due to more individual components needed to support the dual-navigation frequency operations in high-SWaP payload as compared to low-SWaP payload. Higher power requirement also results in bigger and heavier satellite battery system along with higher number of solar cells (the power budget and mass budget along with solar cell calculations is analyzed in more detail in Section V-C and Section V-D respectively).

B. NAVIGATION SIGNAL LINK MARGIN

The link margin is estimated in this work for two navigation frequencies, the L1-band (1576.42 MHz) used by both payload options, and the L5-band (1176.45 MHz) used by only the high-SWaP payload. The summary of the link estimate is shown in Table 13. Dual L-band frequencies provide the advantage of mitigating atmospheric errors while ensuring excellent compatibility and synergy with GNSS MEO satellites. The link budget estimate assumes a bandwidth of 10 MHz based, for example, on our previous studies in [69], a transmit power of 18 W (transmission module input power in Section V-A), a transmitting antenna with isoflux radiation pattern offering 1 dBi gain at nadir (ref. Section IV-E), and an omnidirectional receiver antenna on

ground with 0 dBi gain [41] for each navigation frequency. Furthermore, the satellite is assumed to orbit at an 800 km altitude and have a 30° minimum elevation angle with regard to the ground station. For path loss estimates, a slant range of 1395 km has been considered. The calculated free-space path loss is 156.3 dB for the L5 frequency and 159.8 dB for the L1 frequency. Additional losses include atmospheric effects (e.g., due to clouds and rain) of 0.5 dB for L5 and 1.2 dB for L1, along with a polarization loss of 2.7 dB in both cases. Finally, the estimate assumes the use of a standard advanced matched filter technique in signal processing that improves the link margin by 30 dB. Following these assumptions, the link margin is 10.9 dB and 13.3 dB for the L1-band and L5-band, respectively.

C. SATELLITE POWER BUDGET

The power budget of the whole LEO-PNT satellite is dependent not only on the payload but all other subsystems as well. The subsystems considered for the budget in addition to the payload include the onboard computer (OBC), the attitude determination and control system (ADCS), the propulsion system, the communication system (COM), the electric power system (EPS) and battery. Table 14 shows the estimated satellite power budget for both the low- and high-SWaP cases. The power budget estimate is based on typical power consumption characteristics of subsystems that would fulfill the requirements set by the satellite and payload.

For the power budget estimation, the satellite is assumed to operate in two modes during the mission, nominal mode and maximum power mode. Nominal mode is expected to be active for 99% of the mission lifetime. E.g., the navigation services are offered during nominal mode operations. The maximum power mode is expected to be activated for the remaining 1% of the mission lifetime. Maximum power mode is required primarily for more significant attitude and orbital maneuvers during the mission. The estimated maximum power requirements for the low- and high-SWaP satellites are 92 W and 232 W, respectively. During nominal operations the respective power consumption remains at 93 W and 172 W. Based on the power consumption of the satellite, an estimated total of 210 solar and 420 solar cells would generate 93 W and 235 W to meet the power demands of the low- and high-SWaP satellites, respectively, considering the end-of-life conditions. A 20% margin of safety is assumed for all total power consumption values.

D. SATELLITE MASS BUDGET

Typical mass values of small satellite subsystems can be used to estimate the mass of the LEO-PNT satellite for each payload design. The driving factor of the total satellite mass is the power consumption, which sets the minimum size of batteries and number of solar cells. Based on the selected satellite subsystem and payload masses, the mass of an individual satellite is calculated for both the low- and high-SWaP cases. The power requirements for the nominal mode are the primary drivers of the satellite's mass and size. For the high-SWaP payload, the higher power demand

necessitate more solar cells to generate sufficient power, and larger battery capacity to supply power also when the satellite is in eclipse. Additionally, a heavier satellite requires for more larger and heavier attitude control systems and propulsion systems for attitude and orbit maintenance. These factors add up to result in an estimated mass of 21.23 kg for the low-SWaP satellite and 145.52 kg for the high-SWaP satellite. The details of the mass budget are compiled in Table 15.

E. SATELLITE PLATFORM AND COST ESTIMATE

The size and cost of the satellite platform required to host the proposed LEO-PNT payloads is estimated based on a market survey of available commercial small satellite platforms and their capabilities. The available information of COTS satellite platforms is limited, especially in terms of cost. Nevertheless, tentative estimates based on the market survey findings are presented in the following. The results of the market survey indicate that the low-SWaP payload could be supported by a 12 U COTS CubeSat platform [75]. The high-SWaP payload, on the other hand, would require a significantly (roughly one order of magnitude) heavier COTS platform [76]. As an example, Fig. 5 presents a rendering of the envisioned 12 U satellite with large deployable solar panels for hosting the low-SWaP payload.

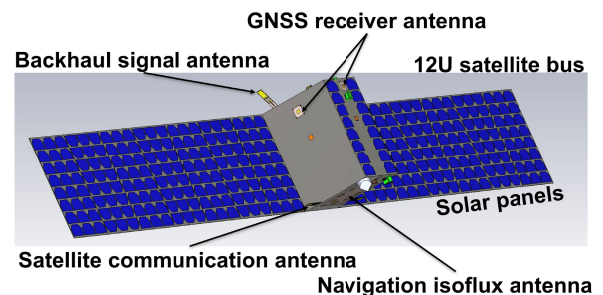


FIGURE 5. A tentative model of the low-SWaP satellite with a 12 U CubeSat structure and large deployable solar panels.

Based on the market survey, the approximate cost of COTS platforms suitable for the low-SWaP and high-SWaP payloads are estimated to be 0.4 M€ and 1.4 M€, respectively. According to the model presented in [79], the payload cost and launch cost can each be estimated to roughly equal the platform cost. This would lead to a total single satellite cost of 1.2 M€ and 4.2 M€ for the low- and high-SWaP systems, respectively.

F. LEO-PNT CONSTELLATION DESIGN

In a recent work by the authors [80], a comprehensive performance analysis of both standalone LEO-PNT constellations and combined LEO-PNT and GNSS systems are presented based on commercial LEO-PNT constellations and GNSS constellations. This work, in contrast, proposes a new Walker Delta LEO-PNT constellation architecture for four-fold global coverage based on optimizing orbital altitude, number of orbital planes and satellites.

TABLE 13. Transmitted navigation signal link margin estimate.

Payload	Frequency band	Frequency (MHz)	Bandwidth (MHz)	TX power (W)	TX antenna gain (dBi)	RX antenna gain (dBi)	Link margin (dB)
Low SWaP	L1	1576.42	10	18	1	0	10.9
High SWaP	L1	1576.42	10	18	1	0	10.9
	L5	1176.45	10	18	1	0	13.3

TABLE 14. Power budget estimate for low- and high-SWaP payload navigation satellite.

Subsystem	Low-SWaP system		High-SWaP system		Ref.
	Max. power consumption (W)	Nominal power consumption (W)	Max. power consumption (W)	Nominal power consumption (W)	
OBC	2.3	2.3	2.3	2.3	[70]
ADCS	15.0	15.0	48.0	48.0	[71]
Propulsion	7.5	0.0	50.0	0.0	[72]
COM	15.0	15.0	15.0	15.0	[73]
EPS and battery	0.1	0.1	0.6	0.6	[74]
Payload	36.0	36.0	77.0	77.0	-
Total (no margin)	76.9	68.4	192.9	142.9	-
Total (20 % margin)	91.1	82.1	231.5	171.5	-

TABLE 15. Mass budget estimate for low- and high-SWaP payload satellites.

Subsystem	Mass (kg)		Ref.
	Low-SWaP	High-SWaP	
OBC	0.11	0.11	[70]
ADCS	0.31	0.97	[71]
Propulsion	0.90	1.20	[72]
COM	0.18	0.18	[73]
EPS and battery	7.07	16.20	[74]
Payload	1.12	2.61	-
Structure	8.0	100.0	[75]–[78]
Total (no margin)	17.7	121.3	-
Total (20 % margin)	21.2	145.5	-

Antenna radiation pattern and beamwidth are some the key factors affecting the number of satellites required for global coverage while ensuring satisfactory C/N_0 . Therefore, the constellation analysis of this work accounts for a realistic isoflux navigation antenna pattern (see Section IV-E), which enables more accurate modeling of practical LEO-PNT constellations. To ensure uninterrupted navigation signals, an overlap of 20% between the ground projections of the navigation antenna radiation patterns are considered for the signal coverage estimates of this work.

The optimized constellation coverage is illustrated in Fig. 6. It is obtained with a single layer Walker Delta

configuration consisting of six orbital planes at an inclination of 55° and 22 satellites per orbit. The constellation provides four-fold satellite coverage globally (from 75°S to 75°S) as required in this work.

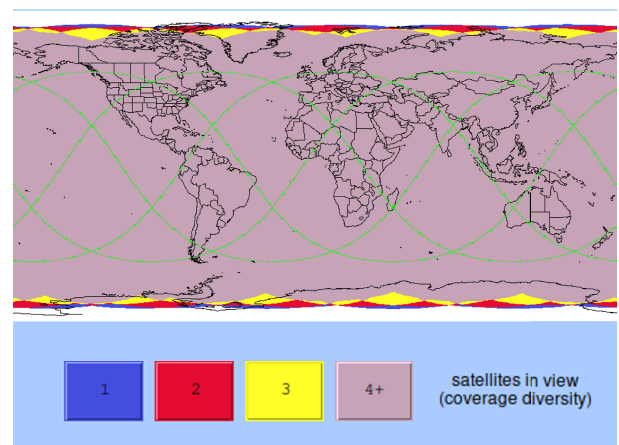


FIGURE 6. Coverage provided by the proposed LEO-PNT constellation. The map is colored according to the number of visible satellites. Blue, red, yellow, and pink correspond to 1, 2, 3, and 4+ simultaneously visible LEO-PNT satellites. The constellation can provide four-fold coverage between the latitudes 75°S to 75°N, as required in this work.

Fig. 7 shows the proposed Walker Delta constellation along with the constellation size dependence on orbital altitude. Below 800 km orbital altitude, the required number of satellites starts growing at an increasing rate. Therefore, 800 km was selected to provide the best compromise between

constellation size and signal strength. Future work can be extended by optimizing the number of satellites using multi-layer orbital planes with varying inclinations to achieve similar results with fewer satellites while also enhancing coverage in polar regions.

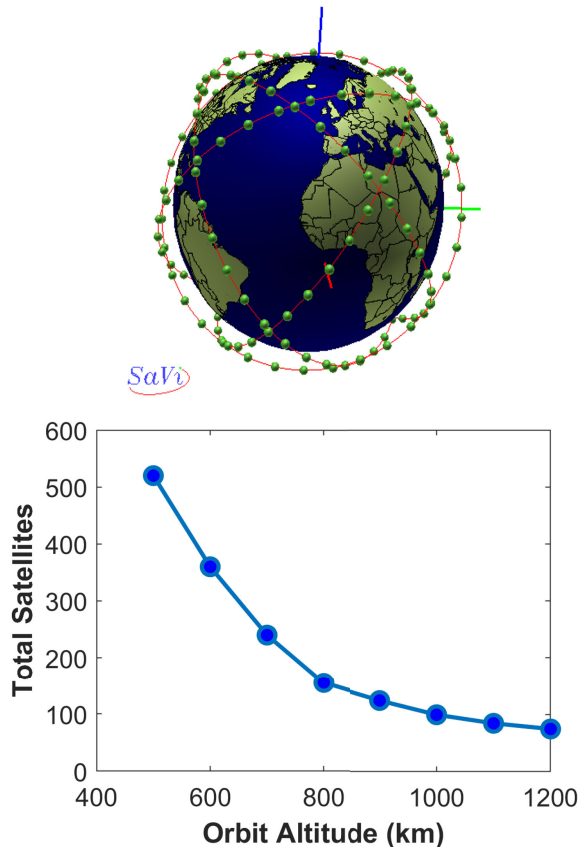


FIGURE 7. Proposed Walker Delta constellation with 800 km orbit and the relation between constellation size and the orbital altitude.

VI. PAYLOAD PERFORMANCE ANALYSIS

This section compares the payload performance in the low- and high-SWaP cases. The key performance parameters considered in this section are the time stability and carrier-to-noise ratio of the payloads.

A. TIME STABILITY

The performance of the time synchronization module for the low- and high-SWaP payloads is presented in Fig. 8. The low-SWaP payload utilizes a CSAC due to its low power demand of 0.12 W and mass of 35 g. The clock offers short term stability in the order of 10^{-10} and medium term stability in the order of 10^{-11} . The high-SWaP payload, in contrast, employs two redundant atomic clocks: a USO ensuring high short-term stability (10^{-13}) and an RAFS providing excellent medium-term stability 10^{-14} . Together, the two atomic clocks are able to offer significantly higher time stability than the CSAC of the low-SWaP payload. The drawback of the better time

stability is the higher power consumption, mass and system complexity of the dual-clock system.

Assuming a 1 ns acceptable limit for the clock deviation over time, it is estimated that the low-SWaP payload can operate autonomously without GNSS signal for up to 100 minutes (roughly equal to one orbital period in LEO) while the high-SWaP system can offer autonomy for up to 24 hours. The lower time stability of the low-SWaP payload makes it significantly more dependent on GNSS infrastructure in space since GNSS signals can be received every 6 seconds.

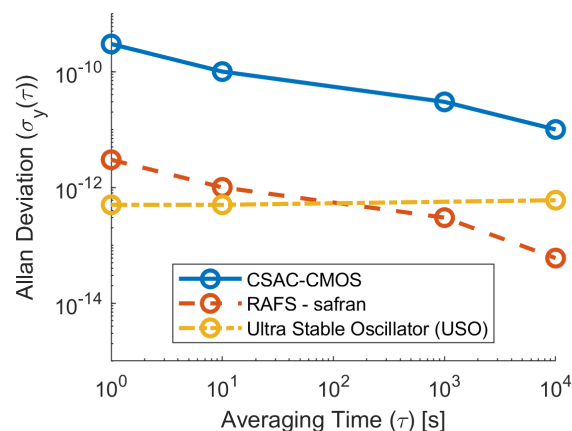


FIGURE 8. Low-SWaP and high-SWaP time synchronization module performance comparison. The low-SWaP module relies on the chip-sized atomic clock (CSAC), whereas the high-SWaP payload utilizes a redundant combination of a rubidium atomic frequency standard (RAFS) and an ultra-stable oscillator (USO).

B. POSITIONING ACCURACY

The positioning performance of any PNT system is typically evaluated through 1) the carrier-to noise ratio (C/N_0), 2) the Dilution of Precision (DOP) and 3) the User Ranging Estimation Error (UERE), assuming a pseudorange-based solution. In this work, the PNT solution is assumed to be performed for a commercial receiver, and thus without external error corrections and with relatively low complexity.

Hence, to evaluate the positioning performance, the C/N_0 of the LEO-PNT payload is analyzed for both projected operating frequencies, i.e., the 1575.42 MHz L1-band (low- and high-SWaP payloads) and the 1175.45 MHz L5-band (high-SWaP payload). The C/N_0 of L1 and L5 band signals as a function of different elevation angles with an assumed 800 km orbital altitude is presented in Fig. 9. The figure shows also the typical C/N_0 of GNSS signals on the ground for comparison. The figure reveals that LEO-PNT satellites are estimated to provide up to more than 10 dB improvement to the C/N_0 compared to GNSS. This suggests that LEO-PNT navigation signals could demonstrate enhanced resilience against signal interference issues (such as signal jamming and spoofing), making navigation services from LEO-PNT satellites more reliable for critical applications.

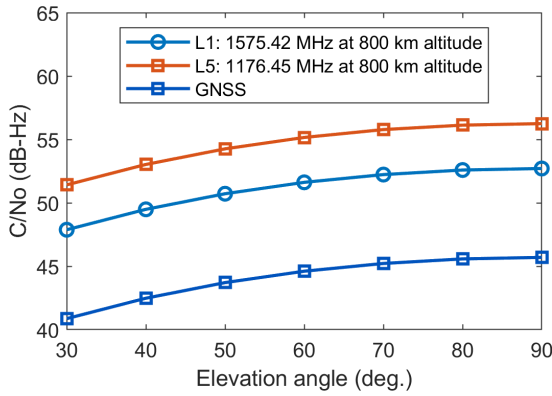


FIGURE 9. Carrier-to-noise ratio for L1- and L5-band signals as a function of the signal elevation angle with an 800 km orbital altitude.

The C/N_0 value can be further improved at lower elevation angles by employing isoflux antennas. As explained in Section IV-E, an isoflux radiation pattern provides higher signal gain at the outer edges of the coverage area. This compensates for the additional signal path loss and improves signal strength at lower elevation angles, thereby enhancing overall performance.

Given that the same transmission power of 18 W is assumed at both carrier frequencies, the C/N_0 performance differences are determined by the orbital altitude of the satellite and the elevation angle of the signal. The orbital altitude and elevation angle define the distance between the satellite and ground terminal, which determines the magnitude of signal path loss. In addition, the elevation angle affects also the quantity of atmospheric attenuation and noise added to the signal.

Fig. 10 presents the C/N_0 for L1- and L5-bands at 30° and 90° elevation angles as a function of the satellite orbital altitude. The lower L5-frequency demonstrates higher C/N_0 due to reduced signal path loss and atmospheric attenuation. The approximately 44 dB-Hz C/N_0 of a typical GNSS signal [81] is also plotted for comparison in the figure. In the case of LEO-PNT signals, both at the L1- and L5-bands, the C/N_0 remains above 50 dB-Hz for orbital altitudes up to 1300 km. At lower altitudes, even up to more than 60 dB-Hz C/N_0 could be reached. This indicates that LEO-PNT satellites can provide a higher C/N_0 than typical GNSS systems from a wide range of different low Earth orbits.

By utilizing higher gain isoflux navigation antennas for LEO-PNT satellites, the C/N_0 could be even further improved. However, increased navigation antenna gain could also result in narrower antenna beams and field-of-view, resulting in a higher number of satellites needed for global coverage.

Next, an analysis of the Geometric DOP (GDOP) is presented for the constellation and scenario described in Section V-F, which was done by simulating 400 users uniformly distributed globally, for 50 different time instances of satellite positions on sky; these time instances are

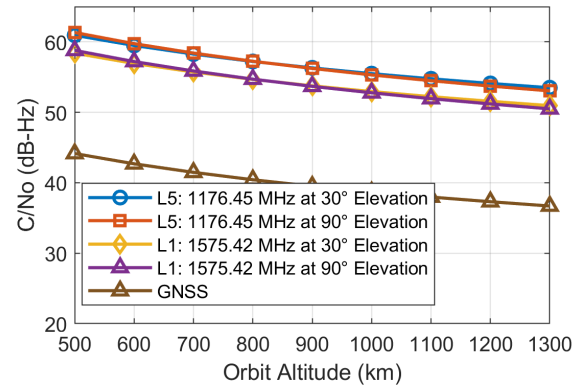


FIGURE 10. C/N_0 of L1- and L5-band signals at low and high elevation angles as a function of orbital altitude compared to typical GNSS C/N_0 magnitude. The model assumes an ideal isoflux radiation pattern for the navigation signal antenna.

separated by 120 seconds, encompassing thus 1.67 h of orbit propagation. The analysis herein considers only the geometric distribution of the visible satellites, and it is not delimited by the receiver sensitivity. Hence, both low-SWaP and high-SWaP solutions will yield the same GDOP values.

This analysis results in GDOP values predominantly ranging between 1.5 and 4, with their average plotted in Fig. 13. The differences in GDOP of the similarly-sized constellations come mainly from the diverse orbital inclinations in their design, but also from the specific navigation antennas proposed in this work. The simulated GDOP values for the proposed constellation demonstrate that high accuracy is achievable, even if these values are worse than those in GNSS.

Finally, the UERE from any received signal typically depends on 1) the received signal noise, 2) the clock and orbit determination errors, 3) the ionospheric error and 4) the tropospheric error [82]. These errors can be reduced by the use of external corrections, by applying techniques such as Precise Point Positioning (PPP) or Real-Time Kinetics (RTK), but these are not applied in most commercial receivers due to their complexity, and are thus not considered in this work. The contribution of each error is described next for GNSS and the proposed LEO payloads:

- GNSS: The UERE is typically in the range of 2 to 10 m in open-sky conditions, although this error varies significantly due to many factors [82]. These errors are typically in the range of 0.4 to 1 m for the satellite clock and orbit, from 0.5 to 3 m for the ionosphere [83], around 0.5 m for the troposphere and 0.5 m for the receiver noise [82].
- Proposed low-SWaP LEO-PNT: Similar errors to GNSS can be assumed for the ionosphere and troposphere, given that the proposed altitude of 800 km is above most of the layers of the ionosphere that produce the strongest degradation of the signal [84]. The clock error will be higher than GNSS, due to the lower quality of the clock. The work in [85] suggests values around 30 m of error

for CSAC clocks, given the high Allan variance shown in Fig. 8, but significantly lower values should be expected when assuming that a GNSS receiver is placed on-board the LEO satellite to synchronize the LEO satellite to the GNSS time. The noise error will be considerably lower due to the 10 dB gain in C/N_0 [86]. These error contributions will lead to lower accuracy than GNSS, but still below the 10 m mark in average.

- Proposed high-SWaP LEO-PNT: Due to the dual-frequency mode of this setup, ionospheric corrections can be applied that effectively lead to a very low ionospheric impact [87]. Furthermore, due to the higher-quality clocks and still assuming the placement of a GNSS receiver on the LEO satellite, the clock error will only be slightly higher than that of GNSS, which might be compensated by the lower noise error from the higher C/N_0 . Hence, the UERE contributions will be similar to those of dual-frequency GNSS, but with stronger resilience to interferences and spoofing.

VII. DISCUSSION

The concept of LEO-PNT has been a topic of active research during recent years, and several companies plan or develop LEO-PNT constellations today. In this section, the low- and high-SWaP LEO-PNT concepts are compared to planned or existing LEO-PNT constellations and satellites. The most prominent modern LEO-PNT constellations that have reached a commercial development stage are briefly described and their SWaP characteristics are presented for comparison. The performance comparison presented here does not include the navigation service performance (signal strength, time stability and link margins) due to the lack of publicly available information of the commercial systems. Hence, the comparison is limited to SWaP estimates which is sufficient to validate that the findings of this work are comparable to commercial state-of-the-art developments. These LEO-PNT constellations are primarily based in the US, China, and Europe.

In the US, Iridium Next [88] offers PNT services in the L-band, featuring 30 dB signal power and 5.2 MHz bandwidth. Similarly, PULSAR by Xona Space Systems [89] plans to operate in the L-band frequencies. TrustPoint, another US-based initiative, aims to provide PNT services in the S- and C-bands using a low-cost 16 U satellite [5]. GlobalStar offers also opportunities for LEO-PNT [90]

In China, Centispace [18] is funded by Chinese entities and operates a dual-frequency system in the L-band with signal power comparable to GNSS. Another Chinese private initiative, Geespace [91], is presumed to be targeting the L-band for its PNT services. In Europe, IRIS² [92] and OneWeb [93] are two prominent initiatives. However, since both projects are in early development stages, their targeted services and frequencies are not yet conclusively defined.

Fig. 11 compares the constellation parameters of this work and the commercial LEO-PNT constellations described above. Compared to the other constellations, the one proposed in this work targets a relatively low orbit. Only one

of the constellations, the Chinese Geespace, is targeting a lower orbit, while the rest are planning or using a similar or higher orbit compared to the constellation of this work.

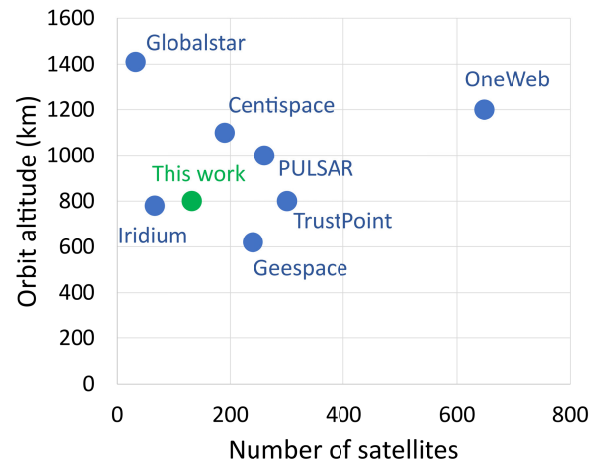
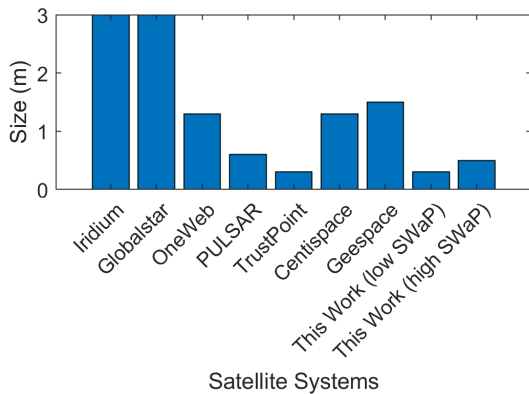


FIGURE 11. Comparison of orbits and numbers of satellites of planned LEO-PNT constellations as recently compiled in [5]. The constellation design proposed in this work is identical in the low- and high-SWaP cases.

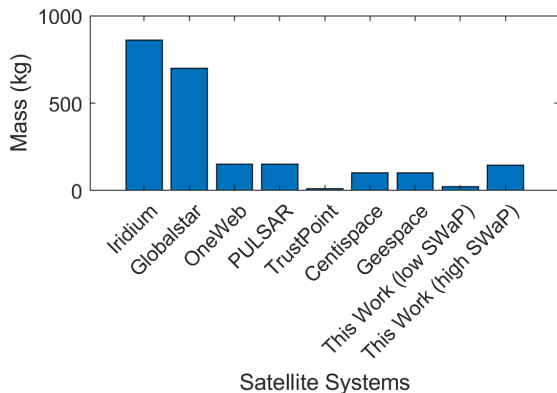
Comparing the number of satellites in the constellations shows that, despite the low orbit, the proposed constellation requires a relatively low number of satellites. For constellations with similar orbits, i.e. Iridium Next and TrustPoint, Iridium Next presents a significantly lower number of satellites, but this is due to their requirement of only single satellite coverage [88], in contrast to the four-fold coverage required of the constellation proposed in this work.

On the other hand, the TrustPoint constellation that also utilizes a similar orbit requires significantly more satellites compared to the proposed constellation. This difference is presumably primarily attributed to the lower navigation antenna beamwidth of the TrustPoint satellites compared to the 100° isoflux beamwidth shown feasible for this work. A narrower beamwidth leads to less ground coverage area per satellite, which again increases the required number of satellites. In fact, based on the navigation antenna dimensions and operating frequency provided by TrustPoint [94], it is possible to present a first order estimation of the TrustPoint antenna beamwidth [95] suggesting it is approximately 40°. This supports the assumption that the larger number of satellites required is due to the significantly narrower antenna beams of the TrustPoint satellites.

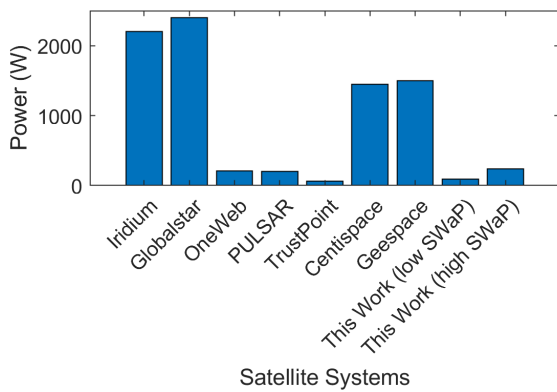
Fig. 12 presents a SWaP comparison of the LEO-PNT satellite proposed in this work and the commercial LEO-PNT projects. When interpreting the differences in SWaP, it should be noted that the PNT performance of the satellites, a key driving factor of SWaP characteristics, is not considered in the figures. Moreover, some of the constellations are not solely dedicated to provide PNT services but also other satellite connectivity services, which can increase the SWaP of the satellites.



(a) Satellite size comparison.



(b) Satellite mass comparison.



(c) Satellite power comparison.

FIGURE 12. SWaP comparison of current and planned state-of-the-art LEO-PNT projects and this work. The compared satellite features are (a) satellite size, (b) satellite mass, and (c) satellite power consumption. The commercial constellation SWaP are as recently compiled in [5].

As Fig. 12 shows, the SWaP characteristics of the low- and high-SWaP satellites proposed in this work resemble most the TrustPoint and PULSAR constellations, respectively. Both these commercial constellations are dedicated for LEO-PNT. Partial agreement in terms of SWaP is observed with certain projects such as OneWeb and Geespace, where some SWaP and constellation parameters align with the design presented

in this work while others do not. Constellation projects such as Iridium and GlobalStar exhibit least correspondence with this work due to their significantly higher SWaP and different constellation parameters.

The SWaP differences could be explained for instance by different coverage requirements, different levels of multi-frequency operations [96], and the varying complexity of the antenna systems of the other constellations and their satellites [97], [98]. Moreover, constellations not dedicated for LEO-PNT, such as Iridium Next and GlobalStar [88], [90], present increased SWaP presumably also due to requirements arising from their various other use cases such as telecommunication. In general, the SWaP characteristics of the LEO-PNT systems proposed in this work correspond best to the SWaP characteristics of other dedicated LEO-PNT constellations.

The GDOP performance of the proposed LEO-PNT constellation is compared to alternative LEO constellations that are at least partly dedicated to PNT applications in Fig. 13. The figure shows that the GDOP performance generally improves with an increasing number of satellites in a constellation. Relatively small constellations such as Iridium, Astrocass and BlackSky, which consist of less than 100 satellites, exhibit higher GDOP and provide more limited ground coverage. The larger constellations (such as TrustPoint, PULSAR, and OneWeb), in contrast, provide significantly better GDOP. The LEO-PNT system proposed in this work can reach GDOP performance comparable to many of the larger constellations even while utilizing a relatively low number of satellites. The excellent performance of the proposed system is enabled by the use of the wide field-of-view isoflux navigation antennas that improve the ground coverage of the satellites. The GDOP accuracy could be further improved by using lower frequency signals, for example in the UHF band.

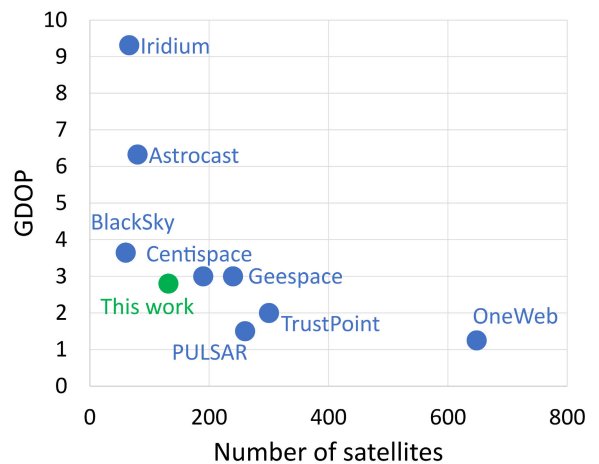


FIGURE 13. Average GDOP of the proposed LEO-PNT satellite constellation compared to selected commercial LEO constellations that are at least partially dedicated for LEO-PNT applications.

Although the above comparison focuses on commercial constellations at least partly dedicated to LEO-PNT, there are also various opportunistic approaches to use LEO constellation not dedicated for PNT for positioning purposes. As a prominent example, the Starlink constellation is demonstrated to be highly suitable for providing signals of opportunity for positioning applications with down to 0.5 m positioning accuracy. The high positioning accuracy based on signals of opportunity can be attributed to the very high number of satellites (more than 11 000) in the Starlink constellation [99].

In addition to positioning accuracy, the time accuracy of the system proposed in this work has been compared to both LEO-PNT constellations with available time accuracy data and GNSS. The time accuracy of the low- and high-SWaP satellites with the proposed constellation is estimated to be 40 ns to 100 ns and 10 ns to 25 ns, respectively, depending on the receiver at the user end. The comparison to other systems is presented in Fig. 14. Since, only few commercial LEO-PNT constellations share their time accuracy performance, only limited comparison to these constellations in terms of time accuracy can be performed. The comparison shows that both systems proposed in this work outperform the 100 ns time accuracy of the Iridium constellation, since Iridium satellites do not carry on-board atomic clocks. On the other hand, Pulsar utilize RAFS [100] and can therefore achieve a high time accuracy of 10 ns [101], on par with the performance with the high-SWaP system performance. The proposed low-SWaP system cannot reach the time accuracy of different GNSS systems, but the high-SWaP option can outperform the time accuracy of Galileo, GLONASS, and BeiDou to reach similar timing accuracy as GPS.

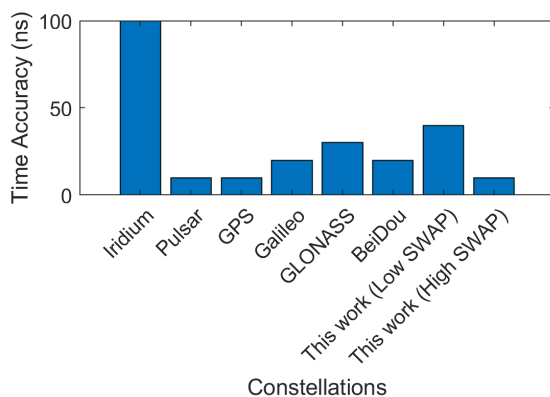


FIGURE 14. Time accuracy comparison of Low- and high SWaP compared to selected LEO-PNT and GNSS constellations.

VIII. CONCLUSION

This work introduces a LEO-PNT navigation payload and satellite concept specifically developed on the basis of an extensive review of commercially or academically available data of instruments and components suited for LEO-PNT applications. The work analyzes the performance of two systems with different SWaP parameters and presents a

satellite platform design able to support the proposed payloads. In addition to the PNT payload and satellite, the work presents a constellation analysis and design that accounts for modeled navigation antenna characteristics.

The key measure used to evaluate the PNT signal quality of the proposed payloads is the carrier-to-noise ratio. The value of C/N_0 is inversely proportional to the altitude of the constellation, making lower orbits more attractive from the PNT service perspective. In the case of the payloads proposed in this work, the C/N_0 values increase from 51 dB-Hz to 57 dB-Hz when decreasing the orbital altitude from 1300 km to 600 km.

In comparison, the typical GNSS signal from MEO has a C/N_0 of 44 dB-Hz, which suggests that the LEO-PNT signals can be stronger than traditional GNSS signals in a wide range of constellation altitudes. The higher C/N_0 of LEO-PNT signals suggest that they are more resilient against interference. In addition, the high-SWaP payload can be expected to provide even higher resilience compared to the low-SWaP payload due to its dual-frequency operation that improves the capability to perform error correction for effects arising from signal propagation in the ionosphere and troposphere, as well as multipath effects. The 800 km LEO-PNT constellation altitude selected in this work is considered a good compromise when balancing the constellation complexity and size against the navigation signal strength and quality.

In addition to the signal power and quality, the clock stability of the payloads is one of the most critical factors in determining the PNT performance. The CSAC time standard used by the low-SWaP payload cannot provide high medium-term time stability, and provides thus constellation autonomy for only up to 100 minutes before the time error accumulation exceeds the allowable 50 ns limit. In contrast, the high-SWaP payload ensures both short-term and medium-term stability by utilizing a CMCU that combines USO and RAFS clocks. A RAFS for LEO-PNT is recommended for better accuracy and increased autonomy. As a result, the high-end payload can offer constellation autonomy for up to 24 hours. It is evident, that the low-SWaP payload is significantly more dependent on the MEO GNSS infrastructure compared to the high-SWaP system. However, both systems are capable of sufficient autonomous operations considering that GNSS signals can be nominally received every 6 seconds, ensuring the critical time stability of both payloads.

The final decision to implement a LEO-PNT satellite constellation does not, however, rely solely on the technical performance of the satellites. It is also critical that the cost of the constellation does not exceed the expected benefits. This work provides a tentative first order estimate of the satellite cost, including payload, platform, and launch. The estimated total cost per satellite is approximately 1.2 M€ and 4.2 M€ for the low- and high-SWaP systems, respectively. The corresponding total cost estimates of the 320 satellite constellation can be approximated by multiplying the satellite cost with the number of satellites to get 380 M€ and 1340 M€. While the estimated constellation cost is large, the

funding for such a LEO-PNT constellation could potentially be feasible considering the ongoing mega-constellation trend.

The proposed LEO-PNT satellite is also compared with prominent commercial LEO-PNT constellation projects. The proposed PNT satellite and constellation design are on a general level aligned with existing projects, which provides some level of validation to the designs of this work. Roughly, the closer the constellation parameters of the existing constellations are to the ones proposed in this work, the better also the SWaP characteristics match. The constellation and satellite comparisons of this work are, however, only indicative, because any PNT performance differences were not considered, and for some of the commercial constellations PNT services might not be the only or even primary function.

As a conclusion, the two proposed LEO-PNT system concepts present significantly different SWaP and cost requirements, but they can both offer improvements compared to current GNSS services. All the payload design objectives were met and demonstrated in the work presented. The concepts can be considered feasible with the technology commercially available today, and the next steps towards the first extensive LEO-PNT constellation could be taken by the implementation of an in-orbit demonstration. Additionally, the results presented in this work can serve as a basis for other realistic simulations of practical LEO-PNT system designs in future studies.

REFERENCES

- [1] L. Ries, M. C. Limon, F.-C. Grec, M. Anghileri, R. Prieto-Cerdeira, F. Abel, J. Miguez, J. V. Perello-Gisbert, S. D'Addio, R. Ioannidis, A. Ostilio, M. Rapisarda, R. Sarnadas, and P. Testani, "Leo-PNT for augmenting Europe's space-based PNT capabilities," in *Proc. IEEE/ION Position, Location Navigat. Symp. (PLANS)*, 2023, pp. 329–337.
- [2] W. Gao, X. Xie, Y. Meng, Q. Li, H. Chen, L. Yang, T. Geng, and Q. Zhao, "Performance analysis of LEO augmented GNSS precise point positioning from in-orbit CENTISPACE™ satellites," *Meas. Sci. Technol.*, vol. 36, no. 1, Jan. 2025, Art. no. 016338. [Online]. Available: <http://iopscience.iop.org/article/10.1088/1361-6501/ad98af>
- [3] N. Jardak, R. Adam, and Q. Jault, "Leveraging multi-LEO satellite signals for opportunistic positioning," *IEEE Access*, vol. 12, pp. 127100–127114, 2024.
- [4] T. E. Bell, "America's other space program: Our military commitment to space is quietly outstripping the civilian NASA program," *Sciences*, vol. 19, no. 10, pp. 6–13, 1979.
- [5] B. Eissfeller, T. Pany, D. Dötterböck, and R. Förstner, "A comparative study of LEO-PNT systems and concepts," in *Proc. ION Pacific PNT*, May 2024, pp. 758–782.
- [6] H. Ge, B. Li, L. Nie, M. Ge, and H. Schuh, "LEO constellation optimization for LEO enhanced global navigation satellite system (LeGNSS)," *Adv. Space Res.*, vol. 66, no. 3, pp. 520–532, Aug. 2020. [Online]. Available: <https://www.sciencedirect.com/science/article/pii/S0273117720302696>
- [7] K. Elikbilek, E. S. Lohan, and J. Praks. (Aug. 2024). *Optimization of a LEO-PNT Constellation: Design Considerations and Open Challenges*. [Online]. Available: <http://dx.doi.org/10.36227/techrxiv.172263277.74357218/v1>
- [8] K. Wang, A. El-Mowafy, and X. Yang, "URE and URA for predicted LEO satellite orbits at different altitudes," *Adv. Space Res.*, vol. 70, no. 8, pp. 2412–2423, Oct. 2022. [Online]. Available: <https://www.sciencedirect.com/science/article/pii/S027311772200775X>
- [9] F. Kunzi, B. Braun, M. Markgraf, and O. Montenbruck, "A GNSS-synchronized satellite navigation payload for LEO PNT," in *Proc. Int. Tech. Meeting Satell. Division Inst. Navigat.*, Oct. 2023, pp. 1425–1435.
- [10] F. Menzione, A. Piccolo, M. Paonni, J. P. Boyero, S. Casotto, M. Bardella, R. Prata, F. J. Belmonte-Calero, M. R. Pérez, D. M. Sanchez, A. Cardeñosa, J. J. L. Bahilo, J. Arias, B. Carreira, C. Cardoso, F. Carvalho, J. Silva, A. Amézcaga, and M. Badia, "Design and testing of NewSpace Galileo receiver for LEO precise onboard orbit determination in the horizon 2020 IOV/IOD mission," in *Proc. 37th Int. Tech. Meeting Satell. Division Inst. Navigat. (ION GNSS+)*, Oct. 2024, pp. 1017–1036.
- [11] C. Chang, Q. Zhao, M. Li, and W. Li, "Augmentation message design for LEO-enhanced precise positioning: in-orbit performance assessment," *Measurement*, vol. 243, Feb. 2025, Art. no. 116314. [Online]. Available: <https://www.sciencedirect.com/science/article/pii/S0263224124021997>
- [12] A. Nardin, F. Dovis, and J. A. Fraire, "Empowering the tracking performance of LEO-based positioning by means of meta-signals," *IEEE J. Radio Freq. Identificat.*, vol. 5, no. 3, pp. 244–253, Sep. 2021.
- [13] F. S. Prol, M. Z. H. Bhuiyan, S. Kaasalainen, E. S. Lohan, J. Praks, K. Çelikbilek, and H. Kuusniemi, "Simulations of dedicated LEO-PNT systems for precise point positioning: Methodology, parameter analysis, and accuracy evaluation," *IEEE Trans. Aerosp. Electron. Syst.*, vol. 60, no. 5, pp. 6499–6516, Oct. 2024.
- [14] Q. Zhang and B. Xu, "Analysis of multipath effects on LEO ranging-based positioning using BPSK and BOC signals in urban areas," *Adv. Space Res.*, vol. 75, no. 3, pp. 3298–3309, Feb. 2025. [Online]. Available: <https://www.sciencedirect.com/science/article/pii/S0273117724011712>
- [15] H. More, E. Cianca, and M. De Sanctis, "Comparing positioning performance of LEO mega-constellations and GNSS in urban canyons," *IEEE Access*, vol. 12, pp. 24465–24482, 2024.
- [16] R. O. Perez, M. C. Limon, P. Giordano, and R. Prieto-Cerdeira, "Mixing real and simulated observables to assess the performance of hybrid GNSS/LEO-PNT precise positioning," in *Proc. Int. Tech. Meeting Satell. Division Inst. Navigat.*, Oct. 2024, pp. 2308–2322.
- [17] N. S. Miller, J. T. Koza, S. C. Morgan, S. M. Martin, A. Neish, R. Grayson, and T. Reid, "SNAP: A xona space systems and GPS software-defined receiver," in *Proc. IEEE/ION Position, Location Navigat. Symp. (PLANS)*, Apr. 2023, pp. 897–904.
- [18] W. Li, Q. Yang, X. Du, M. Li, Q. Zhao, L. Yang, Y. Qin, C. Chang, Y. Wang, and G. Qin, "LEO augmented precise point positioning using real observations from two CENTISPACE™ experimental satellites," *GPS Solutions*, vol. 28, no. 1, p. 44, Jan. 2024.
- [19] Mayank, F. S. Prol, V. Lundén, E. S. Lohan, Z. Saleem, S. Sharma, M. Z. H. Bhuiyan, S. Kaasalainen, H. Kuusniemi, and J. Praks, "LEO-PNT payload architecture and satellite design analysis," in *Proc. IEEE Int. Conf. Wireless Space Extreme Environments (WiSEE)*, Dec. 2024, pp. 124–129.
- [20] F. S. Prol, R. M. Ferre, Z. Saleem, P. Välisuo, C. Pinell, E. S. Lohan, M. Elsanhoury, M. Elmusrati, S. Islam, K. Çelikbilek, K. Selvan, J. Yliaho, K. Rutledge, A. Ojala, L. Ferranti, J. Praks, M. Z. H. Bhuiyan, S. Kaasalainen, and H. Kuusniemi, "Position, navigation, and timing (PNT) through low Earth orbit (LEO) satellites: A survey on current status, challenges, and opportunities," *IEEE Access*, vol. 10, pp. 83971–84002, 2022.
- [21] P. Tavella and G. Petit, "Precise time scales and navigation systems: Mutual benefits of timekeeping and positioning," *Satell. Navigat.*, vol. 1, no. 1, p. 10, Dec. 2020.
- [22] *Department of Defense; United States. Department of Homeland Security; United States. Department of Transportation, United States. Department of Transportation. Office of Positioning, TPMSD of Transportation. Office of the Assistant Secretary for Research, and Technolog*, N United States, Federal radio navigation plan, Washington, DC, USA, Number: DOT-VNTSC-OST-R-15-01, Accessed: Jul. 1, 2022. [Online]. Available: <https://rosap.ntl.bts.gov/view/dot/63024>
- [23] S. Arenas, F. Monjas, A. Montesano, C. Montesano, C. Mangelot, and L. Salghetti, "Performances of Galileo system navigation antenna for global positioning," in *Proc. 5th Eur. Conf. Antennas Propag. (EUCAP)*, Apr. 2011, pp. 1018–1022.
- [24] Microchip. *Csac-sa65*. Accessed: Dec. 12, 2024. [Online]. Available: <https://safran-navigation-timing.com/product/mo-quartz-crystal-oscillator/?modelinterest=MO&productinterest=select>
- [25] Satnow. *Rk409avns*. Accessed: Dec. 12, 2024. [Online]. Available: <https://www.satnow.com/products/oscillators/rakon-limited/129-1392-rk409avns>
- [26] Accubeat. *Ultra Stable Oscillator*. Accessed: Dec. 12, 2024. [Online]. Available: <https://www.satnow.com/products/oscillators/rakon-limited/129-1392-rk409avns>

- [27] Safran. *Minirafs RB Atomic Frequency Standard*. Accessed: Dec. 12, 2024. [Online]. Available: <https://safran-navigation-timing.com/product/minirafs-rb-atomic-frequency-standard/?modelinterest=MiniRAFS&productinterest=singleselect>
- [28] Leonardo. *Mini-PHM*. Accessed: Dec. 12, 2024. [Online]. Available: <https://www.satnow.com/products/atomic-clocks/leonardo/148-1190-mini-phm>
- [29] Phm. Accessed: Dec. 12, 2024. [Online]. Available: <https://electronics.leonardo.com/en/products/phm-1>
- [30] CPU-World. *Nvidia Tegra K1 Sd570n*. Accessed: Dec. 12, 2024. [Online]. Available: <https://www.cpu-world.com/CPU%20s/TegraK1/NVIDIA-Tegra%20K1%20SD570n.html>
- [31] NXP. *Mpc8548e*. Accessed: Dec. 12, 2024. [Online]. Available: <https://www.nxp.com/docs/en/data-sheet/MPC8548EEC.pdf>
- [32] AMD. *Amd Fpga*. Accessed: Dec. 12, 2024. [Online]. Available: <https://www.amd.com/en/products/adaptive-socs-and-fpgas/fpga.html>
- [33] alcatel-alenia space. *Master Clock Unit*. Accessed: Dec. 12, 2024. [Online]. Available: <http://microelectronics.esa.int/mpd2007/ESA2007-NSGU.pdf>
- [34] A. Hauschild, O. Montenbruck, P. Steigenberger, I. Martini, and I. Fernandez-Hernandez, "Orbit determination of sentinel-6A using the Galileo high accuracy service test signal," *GPS Solutions*, vol. 26, no. 4, p. 120, Oct. 2022, doi: [10.1007/s10291-022-01312-5](https://doi.org/10.1007/s10291-022-01312-5).
- [35] F. Kunzi, B. Braun, M. Markgraf, O. Montenbruck, and W. Frese, *First Steps Toward a Fully Operational LEO PNT Payload*. NJ, USA: Inside GNSS, 2024.
- [36] O. Montenbruck, B. Nortier, and S. Mostert, "A miniature GPS receiver for precise orbit determination of the sunsat 2004 micro-satellite," in *Proc. Nat. Tech. Meeting Inst. Navigat.*, Jan. 2004, pp. 636–642. [Online]. Available: <https://www.ion.org/publications/abstract.cfm?articleID=5541>
- [37] P. Kovář, "PiNAV L1—GPS receiver for small satellites," *Gyroscopy Navigat.*, vol. 8, no. 2, pp. 159–164, Apr. 2017, doi: [10.1134/s2075108717020079](https://doi.org/10.1134/s2075108717020079).
- [38] Deimos. *Gnss-G3star*. Accessed: Dec. 27, 2024. [Online]. Available: <https://deimos-space.com/wp-content/uploads/2024/05/Product-G3Star1405.pdf>
- [39] Y. Cai and Z. Wang, "GNSS receiver for Q-Sat and its analysis of precise orbit determination," *Acta Astronautica*, vol. 200, pp. 357–370, Nov. 2022. [Online]. Available: <https://www.sciencedirect.com/science/article/pii/S009457652200443X>
- [40] O. Montenbruck, M. Garcia-Fernandez, and J. Williams, "Performance comparison of semicodeless GPS receivers for LEO satellites," *GPS Solutions*, vol. 10, no. 4, pp. 249–261, Oct. 2006, doi: [10.1007/s10291-006-0025-9](https://doi.org/10.1007/s10291-006-0025-9).
- [41] Anywaves. *Gnss All Bands*. Accessed: Dec. 12, 2024. [Online]. Available: <https://anywaves.com/products/gnss-all-bands-antenna/>
- [42] Taoglas. *ADFGP.60A—Active All Band GNSS High Precision Patch Antenna*. Accessed: Dec. 12, 2024. [Online]. Available: <https://www.taoglas.com/product/allband-gnss-high-precision-patch-antenna/>
- [43] L3harris. *As-48917 Gps Band Omnidirectional Antenna*. Accessed: Dec. 12, 2024. [Online]. Available: <https://www.l3harris.com/sites/default/files/2021-11/AS-48917-Antenna-spec%20sheet-sas-61584-front-digital.pdf>
- [44] Beyond Gravity. *Antennas for GNSS Receivers*. Accessed: Dec. 12, 2024. [Online]. Available: <https://www.beyondgravity.com/sites/default/files/mediadocument/2023-11/Antennas-for-GNSS-receivers.pdf>
- [45] Asartech. *LO1002*. Accessed: Dec. 12, 2024. [Online]. Available: <https://www.asartech.com.tr/wp-content/uploads/2019/09/LO1002v1.3.pdf>
- [46] L. Bagueña, E. Lissoux, J.-M. Dusserre, C. Oustric, P. Bellocq, and V. Heiries, "Development of on board, highly flexible, Galileo signal generator ASIC," in *Proc. ACM Conf.*, Jan. 2007, pp. 679–683.
- [47] Asartech. *SG1001*. Accessed: Dec. 12, 2024. [Online]. Available: <https://www.asartech.com.tr/wp-content/uploads/2019/09/SG1001v1.1.pdf>
- [48] NuWaves. *Multi-Octave RF Upconverter (MORF)*. Accessed: Dec. 12, 2024. [Online]. Available: <https://nuwaves.com/product/multi-octave-rf-upconverter-morf/>
- [49] Mini Circuits. *SSND-6013n-119+*. Accessed: Dec. 12, 2024. [Online]. Available: <https://www.minicircuits.com/pdfs/SSND-6013N-119>
- [50] DST. *DSTRX-1*. Accessed: Dec. 12, 2024. [Online]. Available: <https://satcatalog.s3.us-west-1.amazonaws.com/components/612/SatCatalog-DigitalSignalTechnology-DSTRX-1S-BandTransceiver-Datasheet.pdf?lastmod=20210716010239>
- [51] Endurosat. *S-Band-Receiver*. Accessed: Dec. 12, 2024. [Online]. Available: <https://satcatalog.s3.amazonaws.com/components/1045/SatCatalog-EnduroSat-S-BandReceiver-Datasheet.pdf?lastmod=20210715011936>
- [52] Space-Quest. *Rx-2000 Ceiver*. Accessed: Dec. 12, 2024. [Online]. Available: <https://satcatalog.s3.amazonaws.com/components/1044/SatCatalog-SpaceQuest-RX-2000S-BandReceiver-Datasheet.pdf?lastmod=20210714224308>
- [53] IMT. *C-Band-Transponder*. Accessed: Dec. 12, 2024. [Online]. Available: <https://www.satnow.com/products/transponders/imt/115-1244-c-band-transponder>
- [54] Asartech. *RX1001*. Accessed: Dec. 12, 2024. [Online]. Available: <https://www.asartech.com.tr/wp-content/uploads/2019/09/RX1001v1.3.pdf>
- [55] Reliasat. *TR1000*. Accessed: Dec. 12, 2024. [Online]. Available: <https://reliasat.com/wp-content/uploads/2024/01/TR1000.pdf>
- [56] GomSpace. *Nanocom Sdr Mk3*. Accessed: Dec. 12, 2024. [Online]. Available: <https://gomspace.com/shop/subsystems/communication-systems/nanocom-sdr-mk3.aspx>
- [57] Space-Micro. *USDR*. Accessed: Dec. 12, 2024. [Online]. Available: <https://satcatalog.s3.amazonaws.com/components/681/SatCatalog-SpaceMicro-%C2%B5SDR-C-Datasheet.pdf?lastmod=20210708175945>
- [58] L. Simone, F. de Tiberis, F. Barletta, D. Gelfusa, S. Cocchi, F. Argentieri, R. Viola, I. Martinazzo, M. Delfino, P. Panella, F. Felici, R. Novello, and M. C. Comparini, "A X/X spread-spectrum transponder for secure communication," in *Proc. IEEE Aerosp. Conf.*, Jun. 2006, pp. 1–11.
- [59] Celestial-Space-Technologies-GmbH. *Csr-S-9882-S-Band-Patch-Antenna*. Accessed: Dec. 12, 2024. [Online]. Available: <https://satsearch.co/products/celestial-cst-s-9882-s-band-patch-antenna>
- [60] Anywaves. *S-Band Tr&c Antenna*. Accessed: Dec. 12, 2024. [Online]. Available: <https://anywaves.com/products/s-band-ttc-antenna/>
- [61] V. A. Juarez-Ortiz and R. Perea-Tamayo, "Design of a C-band high gain microstrip antenna array for CubeSat standard," in *IEEE MTT-S Int. Microw. Symp. Dig.*, Dec. 2018, pp. 1–3.
- [62] Reliasat. *Tr500*. Accessed: Dec. 12, 2024. [Online]. Available: <https://reliasat.com/wp-content/uploads/2023/06/TR500.pdf>
- [63] D. Vye, L. Pelletier, S. Steven, D. Aichele, and R. Crampto, "The new power brokers: High voltage RF devices," *Microw. J.*, vol. 52, pp. 22–40, Jan. 2009. [Online]. Available: <https://www.scribd.com/document/91955101/mwj200906-dl>
- [64] Fairview-Microwave. *Fmam5036*. Accessed: Dec. 12, 2024. [Online]. Available: <https://www.digikey.com/en/products/detail/fairview-microwave/FMAM5036/22223070>
- [65] KUHNE-Electronic. *Ku Pa 140150-150 A, Ld-mos Rf Power Amplifier*. Accessed: Dec. 12, 2024. [Online]. Available: <https://shop.kuhne-electronic.com/kuhne/en/shop/industrial/prof-power-amplifier/prof-l-band/KU+PA+140150150+A++LDMOS+RF+Power+Amplifier/?action=shopshowpdfcard&actionid=430&categorylineno=27500>
- [66] RF-Lambda. *RFLUPA01M22GA-Np*. Accessed: Dec. 12, 2024. [Online]. Available: <https://www.rflambda.com/pdf/poweramplifier/RFLUPA01M22GA-NP.pdf>
- [67] V. Lundén, "Optimization of isoflux antenna arrays for small satellites," Aalto Univ., Espoo, Finland, Tech. Rep. URN:NBN:fi:aalto-202408255698, 2024. [Online]. Available: <https://aaltodoc.aalto.fi/handle/123456789/130137>
- [68] S. Li, S. Liao, Y. Yang, W. Che, and Q. Xue, "Low-profile circularly polarized isoflux beam antenna array based on annular aperture elements for CubeSat Earth coverage applications," *IEEE Trans. Antennas Propag.*, vol. 69, no. 9, pp. 5489–5502, Sep. 2021.
- [69] E. S. Lohan and K. Çelikkbilek, "Alternative wireless positioning based on LEO-PNT for low-cost high-accessibility solutions in Africa," in *Proc. IEEE Wireless Commun. Netw. Conf. (WCNC)*, Mar. 2025, pp. 1–6.
- [70] GomSpace. *Nanomind-z7000*. Accessed: Dec. 27, 2024. [Online]. Available: <https://gomspace.com/UserFiles/Subsystems/datasheet/gs-ds-nanomind-z7000-15.pdf>
- [71] Satcatalog. *Cubespace-Gen2-cw0500*. Accessed: Dec. 27, 2024. [Online]. Available: <https://satcatalog.s3.amazonaws.com/components/1403/SatCatalog-CubeSpace-Gen2CubeWheelCW0500-Datasheet.pdf?lastmod=20240627095945>

- [72] Dawnaerospace-b1. Accessed: Dec. 27, 2024. [Online]. Available: <https://satcatalog.s3.amazonaws.com/components/1276/SatCatalog-DawnAerospace-B1Thruster-Datasheet.pdf?lastmod=20220429194702>
- [73] X-link-s-iqspacecom. Accessed: Dec. 27, 2024. [Online]. Available: <https://www.iq-spacecom.com/images/Datasheets/IQspacecomXLink-STM-TCdatasheet02.2024.pdf>
- [74] Titan-2. Accessed: Dec. 27, 2024. [Online]. Available: <https://satcatalog.s3.amazonaws.com/components/1464/SatCatalog-EcuadorianSpaceAgency-TITAN-2BatteryPacksFamily-Datasheet.pdf?lastmod=20240404205046>
- [75] EnduroSat. 12u Platform—next-gen Microsat. Accessed: Nov. 14, 2024. [Online]. Available: <https://www.endurosat.com/products/12u-platform/>
- [76] Endurance-15 Platform—next-gen Espa Class Satellite. Accessed: Nov. 14, 2024. [Online]. Available: <https://www.endurosat.com/products/endurance-15-platform/>
- [77] Dragonfly-Aerospace. Satellite-Bus. Accessed: Jan. 6, 2025. [Online]. Available: <https://www.satcatalog.com/component/dragonfly-bus/>
- [78] SpacemanicCZ. 12usatellite-bus. Accessed: Jan. 6, 2025. [Online]. Available: <https://www.satcatalog.com/component/12u-cubesat-platform-1118-1150/>
- [79] J. D. Liddle, A. P. Holt, S. J. Jason, K. A. O'Donnell, and E. J. Stevens, "Space science with CubeSats and nanosatellites," *Nature Astron.*, vol. 4, no. 11, pp. 1026–1030, Nov. 2020.
- [80] K. Çelikbilek and E. S. Lohan, "A performance study on the combination of available GNSS and potential LEO-PNT constellations," *IEEE Access*, vol. 12, pp. 162909–162917, 2024.
- [81] N. Linty and P. Crosta, "Code and frequency estimation in Galileo mass market receivers," in *Proc. Int. Conf. Localization GNSS (ICL-GNSS)*, Jun. 2013, pp. 1–6.
- [82] K. Borre, I. Fernández-Hernández, J. A. López-Salcedo, and M. Z. H. Bhuiyan, *GNSS Software Receivers*. Cambridge, U.K.: Cambridge Univ. Press, 2022.
- [83] E. S. Lohan and K. Borre, "Accuracy limits in multi-GNSS," *IEEE Trans. Aerosp. Electron. Syst.*, vol. 52, no. 5, pp. 2477–2494, Oct. 2016.
- [84] M. Imad, A. Grenier, X. Zhang, J. Nurmi, and E. S. Lohan, "Ionospheric error models for satellite-based navigation—paving the road towards LEO-PNT solutions," *Computer*, vol. 13, no. 1, p. 4, 2023.
- [85] Z. M. Kassas, N. Khairallah, and S. Kozhaya, "Ad astra: Simultaneous tracking and navigation with megaconstellation LEO satellites," *IEEE Aerosp. Electron. Syst. Mag.*, vol. 39, no. 9, pp. 46–71, Sep. 2024.
- [86] D. Wang and M. Fattouche, "OFDM transmission for time-based range estimation," *IEEE Signal Process. Lett.*, vol. 17, no. 6, pp. 571–574, Jun. 2010.
- [87] G. A. McGraw, P. D. Groves, and B. W. Ashman, "Robust positioning in the presence of multipath and NLOS GNSS signals," in *Proc. Position, Navigat., Timing Technol. 21st Century, Integr. Satell. Navigat., Sensor Syst., Civil Appl.*, Dec. 2020, pp. 551–589.
- [88] G. Kbdy, G. Adamski, and N. May, "Design concepts challenges iridium NEXT command control system," in *Proc. SpaceOps Conf.*, 2018, pp. 1–14. [Online]. Available: <https://arc.aiaa.org/doi/abs/10.2514/6.2018-2708>
- [89] T. G. R. Reid, A. Neish, and B. Manning, "Localization & mapping requirements for level 2+ autonomous vehicles," in *Proc. Int. Tech. Meeting The Inst. Navigat.*, Feb. 2023, pp. 107–123.
- [90] F. Farhangian and R. J. Landry, "High-order pseudorange rate measurement model for multi-constellation LEO/INS integration: Case of iridium-NEXT, orbcomm, and globalstar," *Proc. Inst. Mech. Eng., G, J. Aerosp. Eng.*, vol. 237, no. 4, pp. 925–939, Mar. 2023.
- [91] Geely. *Geely's Satellite Factory Gets the Green Light*. Accessed: Jan. 4, 2025. [Online]. Available: <http://zgh.com/media-center/story/geelys-satellite-factory-gets-the-green-light/?lang=en>
- [92] S. Shankar, "IRIS2: Asserting autonomy in the new space age," *Air Space Law*, vol. 49, no. Issue 6, pp. 547–564, Nov. 2024.
- [93] Y. Henri, "The OneWeb satellite system," in *Handbook of Small Satellites: Technology, Design, Manufacture, Applications, Economics and Regulation*. Cham, Switzerland: Springer, 2020, pp. 1091–1100, doi: 10.1007/978-3-030-36308-6.
- [94] Trustpoint. *Leveraging a Leo Satellite Constellation for Accurate & Reliable Pnt*. Accessed: Jan. 13, 2025. [Online]. Available: <https://www.gps.gov/governance/advisory/meetings/2022-11/shannon.pdf>
- [95] T. A. Milligan, *Modern Antenna Design*. Hoboken, NJ, USA: Wiley, 2005.
- [96] F. J. Dietrich, P. Metzen, and P. Monte, "The globalstar cellular satellite system," *IEEE Trans. Antennas Propag.*, vol. 46, no. 6, pp. 935–942, Jun. 1998.
- [97] P. L. Metzen, "Globalstar satellite phased array antennas," in *Proc. IEEE Int. Conf. Phased Array Syst. Technol.*, Jun. 2000, pp. 207–210.
- [98] J. Schuss, T. Carlson, R. Francois, P. Maloney, A. Rohwer, J. Upton, L. Wardle, and R. Smith, "Design of the iridium phased array antennas," in *Proc. IEEE Antennas Propag. Soc. Int. Symp.*, vol. 1, 1993, pp. 218–221.
- [99] E. Grayver, R. Nelson, E. McDonald, E. Sorensen, and S. Romano, "Position and navigation using starlink," in *Proc. IEEE Aerosp. Conf.*, Mar. 2024, pp. 1–12.
- [100] TeoPortal. *Pulsar*. Accessed: May 12, 2025. [Online]. Available: https://www.eoport.org/satellite-missions/pulsar?utm_source=chatgpt.com#overview
- [101] C. Dalmazzone, M. Guigue, L. Mellet, B. Popov, S. Russo, V. Voisin, M. Abgrall, B. Chupin, C. B. Lim, P.-É. Pottie, and P. Ulrich, "Precise synchronization of a free-running Rubidium atomic clock with GPS time for applications in experimental particle physics," *Nucl. Instrum. Methods Phys. Res. A, Accel. Spectrom. Detect. Assoc. Equip.*, vol. 1075, Jun. 2025, Art. no. 170358, doi: 10.1016/j.nima.2025.170358.



MAYANK received the B.Tech. degree in aerospace engineering from the University of Petroleum and Energy Studies, India, and the M.Sc. degree in space engineering from the Technical University of Berlin, Germany. He is currently pursuing the Ph.D. degree with the School of Electrical Engineering, Aalto University, Finland, focusing on small satellite systems. He has authored two inventions, with one receiving a Finnish patent. His research interests include small satellite communication technologies, navigation systems, and satellite antennas. He was a recipient of the R2B Funding Grant, in 2024, and the IEEE WiSee Best Student Paper Award, in 2024.



F. S. PROL received the Ph.D. degree in cartographic sciences from São Paulo State University (UNESP), Brazil, with a focus on geodetic remote sensing and geodetic positioning, in 2019. He has been with the Finnish Geospatial Research Institute (FGI), since 2021. His research interests include ionospheric modeling, GNSS positioning, and LEO-PNT.



V. LUNDÉN received the B.Sc. (Tech.) degree in electronics and electrical engineering and the M.Sc. (Tech.) degree in microwave engineering from the School of Electrical Engineering, Aalto University, in 2022 and 2024, respectively, where he is currently pursuing the D.Sc. (Tech.) degree in space technology. His research interests include small satellites and satellite antennas and communication technologies. He has been actively involved in several CubeSat projects of Aalto University, where his work has included developing scientific instruments, communication systems, and testing systems.



navigation, and control, with experience across aerospace and robotics.

Z. SALEEM received the bachelor's degree in mechatronics engineering from the University of Sciences and Technology, Pakistan, and the dual master's degree in space science and technology with a major in space robotics from Aalto University, Finland, and Luleå University of Technology, Sweden. She is currently pursuing the Ph.D. degree with the School of Electrical Engineering, Aalto University, working on distributed space systems. Her areas of expertise are guidance,



Finnish universities and other training schools.

M. Z. H. BHUIYAN has been a Technical Expert with the EU Agency for the Space Program (EUSPA) in the H2020 project reviewing and proposal evaluation. He is currently a Research Professor with the Department of Navigation and Positioning, Finnish Geospatial Research Institute. His research interests include multi-GNSS receiver development, PNT robustness and resilience, and seamless positioning. He is actively involved in teaching GNSS-related courses in



GUILLEM FOREMAN-CAMPINS (Graduate Student Member, IEEE) received the M.Sc. degree in telecommunication engineering from the Universitat Autònoma de Barcelona (UAB), in 2022. He is currently pursuing the double Ph.D. degree with Tampere University (TUNI) and UAB, focusing on LEO-PNT. Afterwards, he was with the SPCOMNAV Group, UAB, researching multi-antenna techniques for interference/multipath detection and mitigation for handheld GNSS receivers.



S. KAASALAINEN is currently a Professor and the Head of the Department of Navigation and Positioning, FGI of the National Land Survey. Her research interests include resilient PNT, situational awareness, and optical sensors. She also has research experience in LiDAR remote sensing, sensor development, and astronomy.



H. KUUSNIEMI (Member, IEEE) received the M.Sc. degree (Hons.) in information technology and the Ph.D. degree from Tampere University of Technology, Finland, in 2002 and 2005, respectively. She is currently the Director of the Digital Economy Research Platform and a Professor of computer science with the University of Vaasa, a Research Professor with the Finnish Geospatial Research Institute, National Land Survey of Finland, and an Adjunct Professor in satellite navigation with Tampere University and Aalto University, Finland. She has more than 20 years of experience in research and development of positioning technologies and has held many significant positions of trust and expertise in the global scientific navigation community. Part of her Ph.D. research was conducted with the Department of Geomatics Engineering, University of Calgary, Canada. Her research interests include global navigation satellite systems, especially reliability, estimation, and data fusion, mobile precision positioning with applications, indoor localization, and opportunities of PNT in new space. She was a member of the Research Council for Natural Sciences and Engineering at the Academy of Finland, from 2019 to 2021, and a Visiting Scholar with the GPS Laboratory, Stanford University, in 2017.



S. SHARMA received the Bachelor of Technology degree in electronics and communications engineering from the Indira Gandhi Institute of Technology and the Master of Science degree in space science and technology from Aalto University, where she is currently pursuing the Ph.D. degree. Her areas of expertise is in signal and image processing, digital systems, and flight software.



more than 300 international peer-reviewed publications. Her current research interests include GNSS, LEO-PNT, wireless location techniques, wearable computing, and privacy-aware positioning solutions. She is a Co-Editor of the first book on Galileo Satellite System *Galileo Positioning Technology* (Springer) and a Co-Editor of a book on *Multi-Technology Positioning* (Springer).

E. S. LOHAN (Senior Member, IEEE) received the M.Sc. degree in electrical engineering from the Polytechnics University of Bucharest, Romania, in 1997, the D.E.A. degree (French equivalent of master) in econometrics with the École Polytechnique, Paris, France, in 1998, and the Ph.D. degree in telecommunications from Tampere University of Technology, in 2003. She is currently a Professor with the Electrical Engineering Unit, Tampere University (TAU). She is the author or co-author in



J. PRAKS (Member, IEEE) received the B.Sc. degree in physics from the University of Tartu, Estonia, in 1996, and the D.Sc. (Tech.) degree in space technology and remote sensing from Aalto University, Espoo, Finland, in 2012. He is currently an Assistant Professor of electrical engineering with the Department of Electronics and Nanoengineering, School of Electrical Engineering, Aalto University. He has been working with microwave remote sensing, scattering modeling, microwave radiometry, hyperspectral imaging, and with advanced SAR techniques, such as polarimetry, interferometry, polarimetric interferometry, and tomography. One of the most visited topics in his research is the remote sensing of the boreal forest. Since 2009, he has taken an interest in emerging nanosatellite technology. He led a project that produced the first two Finnish satellites. He has also been involved in spinning off several companies in the field of satellite remote sensing. His research team is a member of the Finnish Centre of Excellence in Research of Sustainable Space and he is a Principal Investigator of several small satellite missions. He is an active member of the scientific community, a member of the Finnish National Committee of COSPAR, the Chairperson of the Finnish National Committee of URSI, and the chair and the co-chair of many national and international conferences.

...